



HAL
open science

Chemical Interactions at the Al/Poly-Epoxy Interface Rationalized by DFT Calculations and a Comparative XPS Analysis

Kanika Anand, Thomas Duguet, Jérôme Esvan, Corinne Lacaze-Dufaure

► **To cite this version:**

Kanika Anand, Thomas Duguet, Jérôme Esvan, Corinne Lacaze-Dufaure. Chemical Interactions at the Al/Poly-Epoxy Interface Rationalized by DFT Calculations and a Comparative XPS Analysis. ACS Applied Materials & Interfaces, 2020, 12 (51), pp.57649-57665. 10.1021/acsami.0c19616 . hal-03153293

HAL Id: hal-03153293

<https://hal.science/hal-03153293>

Submitted on 26 Feb 2021

HAL is a multi-disciplinary open access archive for the deposit and dissemination of scientific research documents, whether they are published or not. The documents may come from teaching and research institutions in France or abroad, or from public or private research centers.

L'archive ouverte pluridisciplinaire **HAL**, est destinée au dépôt et à la diffusion de documents scientifiques de niveau recherche, publiés ou non, émanant des établissements d'enseignement et de recherche français ou étrangers, des laboratoires publics ou privés.







Open Archive Toulouse Archive Ouverte (OATAO)

OATAO is an open access repository that collects the work of Toulouse researchers and makes it freely available over the web where possible

This is an author's version published in: <http://oatao.univ-toulouse.fr/27430>

Official URL: <https://doi.org/10.1021/acsami.0c19616>

To cite this version:

Anand, Kanika  and Duguet, Thomas  and Esvan, Jérôme  and Lacaze-Dufaure, Corinne  *Chemical Interactions at the Al/Poly-Epoxy Interface Rationalized by DFT Calculations and a Comparative XPS Analysis.* (2020) ACS Applied Materials and Interfaces, 12 (51). 57649-57665. ISSN 1944-8244

Any correspondence concerning this service should be sent to the repository administrator: tech-oatao@listes-diff.inp-toulouse.fr

Chemical Interactions at the Al/Poly-Epoxy Interface Rationalized by DFT Calculations and a Comparative XPS Analysis

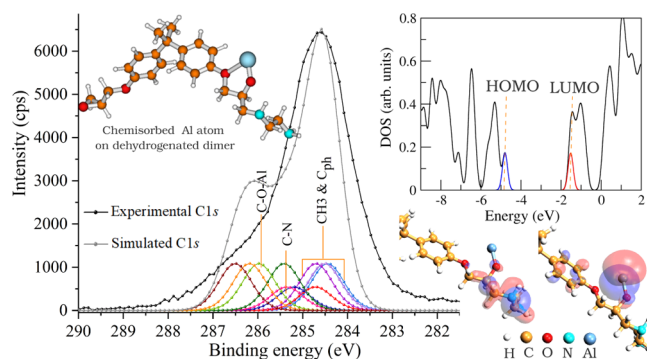
Kanika Anand,* Thomas Duguet, Jérôme Esvan, and Corinne Lacaze-Dufaure

ABSTRACT: A metal–polymer interface is pertinent to numerous technological applications, especially in spatial sectors. The focus of this work is to elaborate on the metallization process of the poly epoxy surface with aluminum thin films, using atomistic details. To this end, X ray photoelectron spectroscopy (XPS) under ultrahigh vacuum and density functional theory calculations are employed. The interfacial bonding between Al atoms and the poly epoxide surface, represented by a dimer model, is studied by determining adsorption energies and by simulating XPS spectra. The latter simulations are mainly performed using the Δ KS method, taking into account the initial and the final state effects. Simulated atom by atom metal deposition on model epoxy systems is attempted to further elucidate energetics of metallization and preferential arrangement of metal atoms at the interface. A fair agreement obtained between XPS experiments and computations rationalizes the interaction mechanism at the atomic scale explaining the formation of the Al/poly epoxy interface. Electronic structure properties highlight the charge transfer from the Al atom(s) to dehydrogenated model epoxy system.

KEYWORDS: epoxy polymers, metal vapor deposition, metal–polymer interface, X ray photoelectron spectroscopy, adsorption, interaction energies, density functional theory, electronic structures

1. INTRODUCTION

Design and tuning of the metal–polymer interface have enabled many technological advancements in the fields of microelectronics, automobile, aerospace, catalysis, and nano medicine.^{1–7} In general, metals and polymers have contrasting properties inducing curiosity about nature of bonds at the interface.⁸ From the past few decades, combined research efforts (both experiment and theory) have been converged on understanding polymer deposition on metal or metal oxide surfaces.^{9–15} On the other hand, metal deposition on polymer surfaces at nanoscale for low regime coverage is still not entirely understood.^{8,16} A useful dimensionless parameter that characterizes the metal–polymer interaction is the condensation coefficient, $C = n_{\text{ads}}/n_{\text{tot}}$ which is defined as the number of adsorbed atoms (n_{ads}) per total number of impinging atoms (n_{tot}). The value C has been experimentally determined to elucidate the interaction between noble metal atoms and the cured epoxy surface.^{17,18} Epoxy polymers and their new derivatives have desirable properties such as high temperature and chemical stability, rapid curing potential, and self healing ability which are applicable in communication systems, wind turbines, and so forth.¹⁹ Metallization of such epoxy polymers have found interest in high performance applications, to withstand drastic conditions.²⁰ Kanzow et al. have described initial stage metal film growth in the case of noble metals such



as Cu, Au, and Ag, which proceeds *via* Volmer–Weber (cluster) mode.¹⁸ Also, at the initial stage of the metal layer formation, a phenomenological approach of progressive chemisorption of Al metal atoms on epoxy resin surfaces is proposed. Furthermore, oxygen atoms belonging to hydroxy or ether groups are suggested as the most probable bonding partners. Indeed, Al among other reactive metals (M) such as Mg, Ca, Cr, Fe, and Ni, is known to form stable oxides and to create strong $(M-O)-C$ bonds.^{21–25}

It has been demonstrated that the strength of the metal reactivity cannot be a sole factor dictating neither the interaction at the metal–polymer interface nor the film growth mechanism.^{26–28} Therefore, the support from theoretical calculations can be crucial to comprehend the experiments related to the metal–polymer interface. A complete description of interfacial bonding at the Al/polyethylene terephthalate (PET, thermoplastic) interface is made possible by combined efforts from experiments (X ray photoelectron spectroscopy,

XPS) and quantum chemical (Hartree–Fock, HF) calculations.²⁹ However, Al/epoxy polymers have been rarely explored using theoretical approaches. Recent work on Cu/poly epoxy (ref 20) has combined the surface science techniques and density functional theory (DFT) calculations to reveal the interfacial bond formation. This combined approach is further extended for the Al/poly epoxy interface while addressing the open questions implied from above discussion. The present study highlights two primary objectives: (i) to understand the local interactions of Al atom(s) with the model epoxy substrate within DFT formalism, accounting for electronic effects; (ii) to expand on the current knowledge of controlled metallization of epoxy based 3D cross linked polymers,^{30–32} through theoretical insights.

In this work, we analyze experimentally a buried interface of Al/poly epoxy through *ex situ* XPS under ultrahigh vacuum (UHV) and atomic force microscopy (AFM) under ambient conditions. Interaction of one Al atom with representative epoxy models is then rendered to identify adsorption sites. We propose a simulated atom by atom deposition on the considered epoxy model systems, constraining to a few adsorbed atoms as we are limited by the size of the model systems. The present study elaborates on metallization energetics to understand experimental XPS results on the buried Al/poly epoxy interface. Further, the charge transfer at the model interface is elucidated. A suitable molecular model is determined through a comparative experimental/theoretical XPS analysis, which is then helpful in revealing interactions at the Al/poly epoxy interface. The discussion section attempts to address some open questions risen in previous works^{18,20} and to illustrate the electronic structure of model epoxy validated by experimental XPS.

2. METHODOLOGY

2.1. Experimental Details. **2.1.1. Preparation of Poly-Epoxy Layer.** In an Ar glovebox, the stoichiometric quantities (2:1) of epoxy resin, diglycidylether of bisphenol A (DGEBA), and curing agent, ethylene diamine (EDA), were slowly mixed in a nonreactive flask to prepare poly epoxy. Then, the clear viscous liquid was placed on the Si wafer to form a thick layer and then left for 24 h for slow polymerization at room temperature. A sufficient thick layer (>300 μm) is required to avoid polymer/Si interphase formation.^{33–36} A couple of hours of postcuring was performed to ensure the depletion of amine from the mixture above the glass transition (140 $^{\circ}\text{C}$) temperature. This complete procedure is detailed in refs^{18,36} and is effective in limiting defects at the surface and in the bulk of the polymer film. The thickness of poly epoxy layer measured using profilometer is 657 μm .

2.1.2. Metallization under UHV. Several tests were performed to calibrate Al source deposition parameters such as source current because of the elemental low partial pressure of aluminum. A pure Al (99.999%) thread was placed in a molybdenum crucible. An e beam evaporator (Mantis M EV) was used in a chamber with a base pressure of 3.0×10^{-10} mbar. During deposition (8 min) at room temperature, the base pressure remained in low 10^{-9} mbar for a source current of 29.5 nA (at 39.9 W). Thus, a uniform and pure thin film of Al was deposited on the pristine polymer surface.

2.1.3. Ex Situ XPS. XPS experiments under UHV were performed with Thermo Scientific K Alpha apparatus using a monochromated Al K α ($E^{\text{Al K}\alpha} = 1486.6$ eV) X ray source. The

pass energy was fixed at 30 eV with a step size of 0.1 eV for core levels. The spectrometer energy calibration was done using the Au 4f_{7/2} (83.9 ± 0.1 eV) and Cu 2p_{3/2} (932.8 ± 0.1 eV) photoelectron lines. Flood gun was used to avoid charging effects at the surface. Ion etching was performed with Ar⁺ ions (1 keV, 10 μA , raster area of 2 mm²) to remove the surface contamination during the transfer to the XPS apparatus and to reach the buried interface. For the latter, we monitored the recovery of metallic aluminum by analyzing the relative intensities of adjacent aluminum oxide and metal aluminum peaks. The shape of the metallic Al 2p peak is also compared with the reference Al foil. The C 1s peak was also constantly monitored. After 110 s of sputtering and careful evaluation of line as well as survey spectra, we could assume that C 1s and O 1s signals originated from the carbon and oxygen of the poly epoxy, respectively, buried underneath the Al film. Therefore, we were able to investigate the interface and evaluate the interfacial bonding through fine decomposition of C 1s and O 1s peaks. For the peak analysis in the present work, a Shirley background was systematically subtracted. Thermo Avantage V. 4.53 was used for fitting and quantification of XPS data.

2.1.4. Atomic Force Microscopy. AFM measurements were performed on Al film deposited on the epoxy polymer under ambient conditions using Bruker Dimension Icon with ScanAsyst, Dektak XT. Peak force tapping control mode was used with a silicon tip (on nitride lever) of $k = 0.4$ N/m (Bruker's model: ScanAsyst Air). The image scanning rate was 0.99 Hz. Post processing of AFM images was achieved through Gwyddion (version 2.56), a scanning probe microscopy tool.

2.2. Computational Details. A molecular (dimer) model was considered to describe the poly epoxy surface (Figure 1).

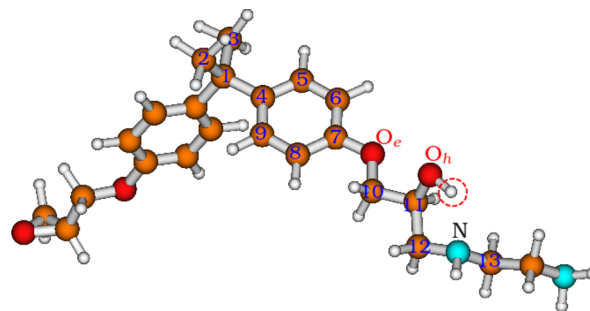


Figure 1. Optimized geometry of dimer (D) model. Encircled H atom is removed in the DwH model. Color code for atoms: C = orange, O = red, N = cyan, H = white; this color code is applicable throughout the present work.

It is composed of one monomer of epoxy, DGEBA, and one monomer of amine, EDA, linked to each other by opening of one oxirane to form a hydroxy group and a C–N bond between them. We considered two models to perform our systematic study of the Al/epoxy polymer interface. One is the native dimer (D) model and other is dehydrogenated dimer (DwH) model obtained by removing hydrogen atom belonging to the hydroxy group, highlighted by the dashed red circle in Figure 1. For DFT calculations (adsorption study or XPS simulation), we took into account only the branch of the epoxy monomer which is attached to the EDA monomer, that is representative of the poly epoxy. The other side is not relevant as it contains the unreacted epoxy group.

2.2.1. Al Adsorption Sites. Many sites were considered for the adsorption of one Al atom on the substrate models. A few

of these adsorption sites (O_e ; O_h ; N) are marked in Figure 1. Various geometries were fully optimized using the Berny algorithm in Gaussian 09.³⁷ The gradient corrected PBE functional³⁸ with and without empirical dispersion correction (GD3)³⁹ was used along with basis set 6-31+G*,^{40,41} that is, polarization and diffusion functions in addition to the set. Also, the calculations were performed using PBE D3 in combination with large basis set def2TZVP.^{42,43} A frequency analysis was carried out to characterize the stable geometries as minima which was followed by natural bond orbital (NBO) charge analysis.⁴⁴ We denote model epoxy systems in interaction with a single Al atom as Al/D or Al/DwH models (Section 3).

2.2.2. Simulated Atom by Atom Deposition. Energetically most stable sites were identified for adsorption of a single Al atom on the proposed substrate models and then atom by atom deposition was executed. In this process, after each new addition of the Al atom, we fully optimized the metal/organic structures. This approach is valuable for understanding interaction or bonding mechanism at the interface as proposed in ref 20. These DFT calculations were performed at the PBE D3/def2TZVP level of theory, accompanied by additional NBO charge analysis. Models showing interaction of more than one Al atom with epoxy substrates are denoted as Al_n/D or Al_n/DwH ($n = 2-4$).

2.2.3. XPS Calculations. Fully optimized geometries obtained using Gaussian 09 were used as input to XPS calculations. These calculations were performed within the framework of ΔKS ⁴⁵⁻⁴⁷ using deMon2K code.⁴⁸ Full reoptimization of molecular structures was again performed using the PBE functional, relativistic basis, and effective core potentials (RECP/SD)⁴⁹ for all atoms excluding H atoms (DZVP) and GENA2 auxiliary functions.⁵⁰ On the most stable Al/D and Al/DwH geometries, simulation of XPS spectra was performed. It accounts for both initial (neutral) and final (ionized) state of the system that can be described as follows:

1. Single point (SP) energy calculations on the optimized geometry of the nonionized system, to obtain the total energy of the system, by using all electron potential and augmented basis set (AUG CC PVTZ)⁵¹ for the atom of interest, that is, C^* denoted hereafter.
2. Similarly, SP calculations for the ionized system with no electron in the α molecular orbital (MO) of the core-shell of C^* .
3. Finally, the binding energy (BE) was calculated using the ΔKS theory⁴⁵⁻⁴⁷ and mathematically represented by the following equation

$$BE = E_{\text{neutral}}^{\text{tot}} - E_{\text{ionized}}^{\text{tot}} \quad (1)$$

where $E_{\text{neutral}}^{\text{tot}}$ and $E_{\text{ionized}}^{\text{tot}}$ are the total energy values of neutral and ionized systems, respectively. The core level chemical shifts (ΔBE) were calculated relative to the lowest BE of the data set. The calculated ΔBE values were used to compose the simulated spectrum, which was then compared with the experimental spectrum.

Additionally, results of calculated BE using the uGTS method as described in⁵²⁻⁵⁴ are available in Supporting Information.

3. RESULTS

3.1. XPS Analysis: C 1s Spectra. Normalized experimental C 1s spectra of the clean epoxy surface (in red) and with Al deposition after 110 s of etching (as filled area) are

presented in Figure 2. The pristine C 1s peak of the poly epoxy surface consists of three prominent components.^{20,55} A main

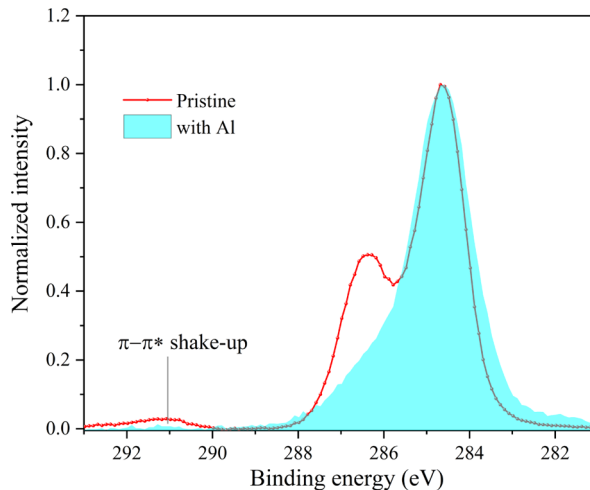


Figure 2. C 1s spectra of the clean (red curve) and Al covered (filled area) poly epoxy surface.

peak centered at a BE of 284.6 eV arises from aliphatic C or aromatic C contributions. A high BE shoulder (at 286.3 eV) presents C–O components and a π – π^* shake up satellite at 291.2 eV.

In the present work, the simulated C 1s spectrum of the representative dimer model using the ΔKS method is shown in Figure S1 and the calculated chemical shift values using both ΔKS and uGTS methods are gathered in Table S1. These values are similar to the previously simulated C 1s using pristine epoxy dimer.²⁰ Also, the experimental O 1s spectrum (black line) of pristine epoxy surface along with the simulated envelope (gray line) using the ΔKS method is presented in Figure S2.

After Al deposition, differences from C 1s of the pristine surface are marked by the diminishing intensity of the high BE shoulder, disappearance of shake up satellite, and the appearance of amorphous carbonaceous components around low BE (282.5 eV) values. The three effects are observed on several heteroatom (N,O) containing polymer surfaces after metal vapor deposition.^{24,56,57}

On comparing the normalized C 1s spectra of Cu/poly epoxy and Al/poly epoxy buried interfaces (Figure S3), we find almost similar peak shapes. Only a slight slant broadening of the main C 1s peak at the disappeared high BE shoulder peak value can be spotted in the case of Al/poly epoxy in comparison to the Cu/poly epoxy buried interface. Because Al is known to be more reactive than Cu atoms, it requires more understanding to explain similarities in their behavior at the interface. Earlier works attempted to correlate distinct aspects of the metal–organic interface with known properties of metal or organic atoms.^{16,58} It can be simply condensation energies (E_{coh}) of metal (for e.g., $E_{\text{coh}}^{\text{Al}} = 3.420$ eV/atom & $E_{\text{coh}}^{\text{Cu}} = 3.472$ eV/atom⁵⁹) or diffusion behaviors at the interface.^{24,58} Thus, a possible explanation can be the lower reactivity of Cu being counterbalanced by its diffusivity into the surface to react with more nucleation sites, whereas Al is reactive but does not diffuse into the polymeric surface. This may imply similar C 1s peaks after deposition of the (Cu or Al) metallic film up to 10 nm thickness. We also observed attenuation of overall intensity of C 1s peaks in both cases which can either be explained as

long exposure to metal vapor deposition²⁴ or to be characteristic of cluster growth as suggested in ref 56 for low metal coverage.

We present Al 2p and O 1s spectra, obtained after 110 s of etching of the Al film, in Figures S4 and S5 of Supporting Information. We observe the oxidized Al peak at 74.1 eV and metal like Al peak at 71.1 eV. The shift with respect to a typical metallic Al peak (72.5 eV¹⁸) can be attributed to the presence of Al clusters at the initial stage of a metal overlayer growth.²⁹ On probing a buried interface, we obtain a rather sharp oxygen peak centered at 531.5 eV. This position of O 1s is known to correspond to the formation of Al–O–C bonds.⁵⁶

3.2. XPS and AFM: Al/Poly-Epoxy. In this work, we are analyzing the buried interface which is accessed by sputtering the Al film deposited on poly epoxy. We find that soft sputtering (1 keV, 10 μ A, 110 s) is appropriate: (i) to remove surface pollution (from exposure to air) and (ii) to obtain a good signal of Al(0) 2p (from Al film) and C 1s (from poly epoxy substrate). A good intensity of the C 1s peak points to the fact that Al film thickness must be less than or equal to 9.4 nm, that is, three times the inelastic mean free path (IMFP or $\lambda = 3.1$ nm⁶⁰) of Al photoelectrons with a kinetic energy of 1416 eV. Further, characterization of the surface of the Al film with AFM provides its morphological aspects and an approximate estimation to its thickness. Figure 3 shows a 500 \times 500 nm² AFM image of the Al film.

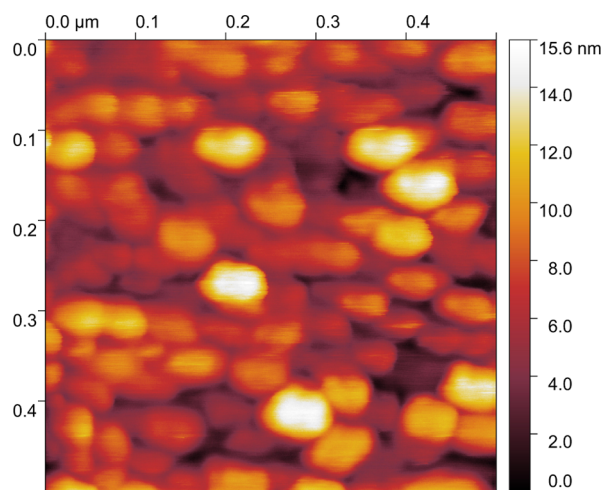


Figure 3. AFM image (500 \times 500 nm²) of the Al film covering the poly epoxy substrate.

The morphology of the Al film consists of small islands or bright three dimensional blobs with a maximum height roughness, $S_z = 15.61$ nm, and peak to peak roughness, $S_p = 8.97$ nm. We also observe some contrasting dark pits that might point to uncovered substrate zones. However, most of the polymeric substrate is covered with the Al film along with its native oxide with mean surface roughness, $S_a = 2.04$ nm. The concomitant aluminum oxide layer is usually found to be 2–4 nm thick under ambient conditions.⁶¹ The quantification of Al 2p metal and oxide peak intensities of the Al film on the poly epoxy sample (after 110 s of etching) gives surface oxide layer thickness, d_{XPS} (nm) = 2.4 nm, as detailed in refs.^{61,62} Thus, by combining XPS and AFM analyses, an estimation of Al film thickness including contribution from the oxide layer present during XPS and then because of additional exposure to air while performing AFM; in this case, it would be 10 ± 3 nm.

3.3. Metallization Energetics. 3.3.1. *One Al Atom on D and DwH Models.* To understand adsorption mechanism and metal–organic interactions, we built different metal/molecular structures pertinent to the present study. In Figure 4, fully

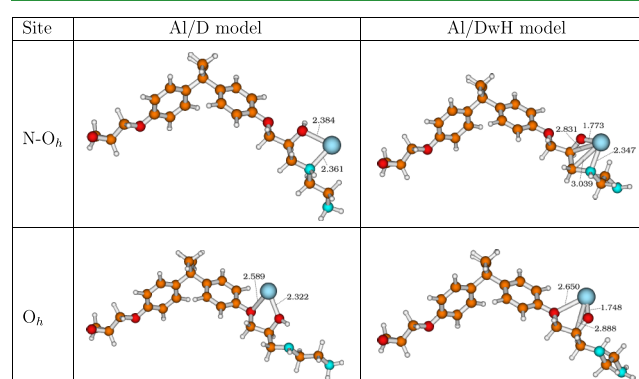


Figure 4. Optimized metal–organic structures representing interaction of the single Al atom with D and DwH dimer models. Shown bond distance values are in Å at the PBE D3/def2TZVP level of theory. The adsorbed Al atom is depicted as the blue sphere.

optimized Al/D and Al/DwH structures corresponding to the stable sites such as O_h and N O_h (between N and O_h) are illustrated. Optimized bond length values inferior to 3.100 Å are also shown. We have chosen this value as the maximum limit, considering the sum of vdW radii of Al atom and either of the organic atoms (C, O, N), that is, ($r_{\text{vdW}}^{\text{Al}} + r_{\text{vdW}}^{\text{C}} = 3.54$ Å; $r_{\text{vdW}}^{\text{Al}} + r_{\text{vdW}}^{\text{O}} = 3.36$ Å; $r_{\text{vdW}}^{\text{Al}} + r_{\text{vdW}}^{\text{N}} = 3.39$ Å).⁶³

For D and DwH models, most of the tested initial geometries converged to either of the two configurations, that is, stable sites, O_h and N O_h. Difference in total energy values of these tested geometries for a particular site of a D or DwH model reaches a maximum value up to 0.010 eV. In the case of the D model, another stable configuration (called as C_{ph} site) is found and is shown in Figure S6. However, the optimized structure shows a slight deformation of the phenyl ring attached to the Al atom. Similar configuration could not be converged in the case of adsorption of Al on the DwH model at the C_{ph} site. Detailed bond distance analysis with values (in Å) for all Al/D or DwH models using PBE D3/(def2TZVP or 6 31+G*) and PBE/6 31+G* functionals is provided in Table S2. The optimized Al–O_h and Al–N distances for Al/D (site = N O_h) are 2.384 and 2.361 Å, respectively, while Al–O_h and Al–O_c bond lengths for Al/D (site = O_h) are 2.322 and 2.589 Å, respectively. Here, these bond lengths suggest an ionic–covalent interaction between the Al atom and native dimer model. The sum of covalent radii of these atoms (*i.e.*, $r_{\text{cov}}^{\text{Al}} + r_{\text{cov}}^{\text{C}} = 1.99$ Å; $r_{\text{cov}}^{\text{Al}} + r_{\text{cov}}^{\text{O}} = 1.88$ Å; $r_{\text{cov}}^{\text{Al}} + r_{\text{cov}}^{\text{N}} = 1.95$ Å)^{59,64} is less than 2.000 Å. The optimized Al–O_h bond lengths at N O_h and O_h sites of Al/DwH model are 1.773 and 1.748 Å, respectively. The latter models show short Al–O bond distances which correspond well with values (calc. = 1.70 Å; exp. = 1.76 Å) reported in earlier works.^{29,65} These bond lengths also indicate covalent bonding between Al and O in the case of Al/DwH models. For Al interaction with C_{phenyl}, average Al–C_{phenyl} distance for the Al/D (site = C_{ph}) model is 2.557 Å and the previously reported value using *ab initio* HF is 2.06 Å.⁶⁶ In the case of the Cu/poly epoxy interface,²⁰ avg. Cu–C_{phenyl} distance was determined to be 1.947 Å. Al interaction with C_{phenyl} in the native epoxy dimer has more ionic character rather than pure covalent as also observed in

the Cu/epoxy study.²⁰ Regarding the Al/PET system (ref 66), Al–metal interaction with C_{phenyl} was found to be possible only for a high metal coverage.

It is important to identify the energetically favorable adsorption sites to comprehend the chemical interactions using Al/D (or DwH) models. Interaction between the Al atom and considered dimer substrate models is defined by the following eq 2.

$$E_{\text{int}} = E_{\text{Al/substrate}}^{\text{tot}} - E_{\text{substrate}}^{\text{tot}} - E_{1\text{Alatom}}^{\text{tot}} \quad (2)$$

where substrate = D or DwH model.

$E_{\text{Al/substrate}}^{\text{tot}}$, $E_{\text{substrate}}^{\text{tot}}$, and $E_{1\text{Alatom}}^{\text{tot}}$ are the total energies of the system (one Al atom adsorbed on the substrate D or DwH model), the pristine dimer (D or DwH) model, and an isolated Al atom, respectively.

The adsorption energy (E_{ads}) for Al/D models, with intact hydroxy (–OH) group in their substrate, is same as the interaction energy (E_{int}) calculated using eq 2. We also considered a scenario in which the native dimer is dehydrogenated (*i.e.*, DwH model) to promote metal adsorption. In such a case, adsorption energy can be determined by considering the dissociation energy of the O–H bond ($E_{\text{diss}}^{\text{OH}}$) and the formation energy of the H_2 ($E_{\text{form}}^{\text{H}_2}$) molecule. Thus, thermodynamically, we can define adsorption energy for the DwH model as

$$E_{\text{ads}} = E_{\text{int}} + E_{\text{diss}}^{\text{OH}} + \frac{1}{2}E_{\text{form}}^{\text{H}_2} \quad (3)$$

where E_{int} is the interaction energy value obtained using eq 2 for DwH as the substrate model.

In the present work, the bond dissociation energy of the O–H bond is calculated using $E_{\text{diss}}^{\text{OH}} = E_{\text{DwH}}^{\text{tot}} + E_{1\text{Hatom}}^{\text{tot}} - E_{\text{D}}^{\text{tot}}$, where the total energy of the dimer, D model, is subtracted from the sum of the total energies of dehydrogenated, DwH model and single isolated H atom.

The values of dissociation energy of the O–H bond and formation energy of the H_2 molecule calculated in this study and proposed in previous works are gathered in Table 1. In ref

Table 1. Dissociation Energy (eV) of O–H Bond and Formation energy (eV) of the H_2 Molecule

$E_{\text{diss}}^{\text{OH}}$	$E_{\text{form}}^{\text{H}_2}$	method (refs)
4.430	4.533	PBE-D3/def2TZVP (this work)
4.335	4.546	PBE-D3/6-31+G* (this work)
4.340	4.546	PBE/6-31+G* (this work)
4.434	4.547	PBE/6-31G* ²⁰
4.575	4.760	B3LYP/6-31G* ²⁰
	4.520	calc. ^{67,68}
	4.740	exp. ⁶⁹
4.454 ^a		exp. ⁵⁹
4.527 ^b ; 4.978 ^c		calc. ^{b70c71}
4.562 ^b ; 5.152 ^c		exp. ^{b70c71}

^aMolecule used: O–H. ^bMolecule used: $\text{CH}_3\text{O–H}$. ^cMolecule used: HO–H.

20, these values were calculated using similar molecular structures but different functional and basis sets. The O–H bond dissociation energy in earlier works were reported using $\text{CH}_3\text{O–H}$ or HO–H with *ab initio*/6 311G(d,p) methods,^{70,71} and the formation energy of H_2 was provided using pseudo potentials and GGA methods.^{67,68} The calculated $E_{\text{diss}}^{\text{OH}}$ (4.430

eV) value (PBE D3/def2TZVP) in this work agrees well with exp. value (4.454 eV).⁵⁹ Although, the O–H bond dissociation energy is sensitive to substituent effects,⁷⁰ that is, to the molecular system used. In this work, calculated $E_{\text{form}}^{\text{H}_2}$ (–4.533 eV) is underestimated compared to the exp. value (–4.740 eV)⁶⁹ but not enough to change thermodynamic conditions.

The values of adsorption energies are presented in Table 2, where all adsorption sites correspond to stable structures for Al adsorption. It is evident from all calculations that there is considerable strengthening in the binding of the aluminum atom on the DwH model compared to the D model. The difference in adsorption energies between the two interface models for the most stable site (N–O_h) is 1.93 eV. In fact, for energetically less favorable site (O_h), the difference remains approximately same. Clearly, the adsorption of Al is facilitated by the departure of the H atom at the O_h site, making the Al/DwH structures the more probable representations from a thermodynamical point of view. For Al/D models, E_{int} values (as defined in eq 2) corresponding to N–O_h, C_{phenyl} , and O_h sites are –0.865, –0.727, and –0.584 eV, respectively. Even when considering either the def2TZVP or 6 31+G* basis set with the PBE D3 functional and PBE/6 31+G*, the order of energetic preference remains N O_h > C_{phenyl} > O_h. Similarly, for the Al/DwH system, calculated E_{int} values (from eq 2), using the PBE D3/def2TZVP (or 6 31+G*) basis set, for N O_h and O_h sites are –4.958 (–4.872) and –4.762 (–4.668) eV, respectively. On using PBE/6 31+G* for Al/DwH models, we obtain E_{int} values equal to –4.813 and –4.577 eV at N O_h and O_h sites, respectively. Comparison between PBE/6 31+G* and PBE D3/6 31+G* using calculated E_{int} values highlights the increase in interaction on considering van der Waal forces (empirical dispersion) at the Al/epoxy interface. There is a conspicuous stronger interaction of the Al atom with the DwH than with the native dimer model. For Al/D models, bond lengths are greater than the sum of covalent radii of atoms in interactions and E_{int} values less than –1.000 eV which suggest physisorption. However, the Al atom is chemisorbed on the DwH model on taking into account both bond analysis and energetics. Between the two stable sites (N O_h and O_h) identified for a given Al/D or Al/DwH model, an adsorption energy difference (ΔE_{ads}) is up to 0.28 eV. It implies a small energy anisotropy at the Al/epoxy interface when compared to the difference being 0.65 eV for the Cu/epoxy interface²⁰ considering the similar sites.

In Table 2, the NBO charges for the Al atom (Q_{Al}) are shown, using PBE D3/def2TZVP or 6 31+G* and PBE/6 31+G* functionals. We observe a little to no charge transfer at N O_h and O_h sites of Al/D models. However, in particular, the Al atom has a net positive charge +0.66 e at the C_{phenyl} site which illustrates its oxidized state. In the case of Al/DwH, Al atoms corresponding to N O_h and O_h sites have +0.71 e and +0.78 e charges, respectively. This is in accordance with less electronegativity of the Al (1.61) atom compared to organic atoms such as O (3.44), N (3.04), and C (2.55); here, bracket values are electronegativity at Pauling scale.⁵⁹ The previous work on the Al/epoxy polymer interface also suggests Al atoms as the e donor while atoms in its vicinity as the e acceptor.⁸ Also, for the Al/PET interface (ref 29), an average charge of +0.55 e was found on Al atoms, considering various geometries. NBO charge analysis underlines physisorption for Al/D models and chemisorption for Al/DwH models at N O_h and O_h sites.

Table 2. Adsorption Energies (in eV) and NBO Charges (in e) on the Al Atom

	adsorption site	^a E_{ads}	^b E_{ads}	^c E_{ads}	^a Q_{Al}	^b Q_{Al}	^c Q_{Al}
Al/D	N O_h	0.865	0.914	0.830	0.08	0.07	0.06
	O_h	0.584	0.624	0.519	+0.02	+0.00	+0.00
	C _{phenyl}	0.727	0.675	0.628	+0.66	+0.65	+0.64
Al/DwH	N O_h	2.795	2.810	2.746	+0.70	+0.71	+0.71
	O_h	2.599	2.605	2.511	+0.79	+0.78	+0.78

^aAt the PBE D3/def2TZVP level of theory. ^bAt the PBE D3/6 31+G* level of theory. ^cAt the PBE/6 31+G* level of theory.

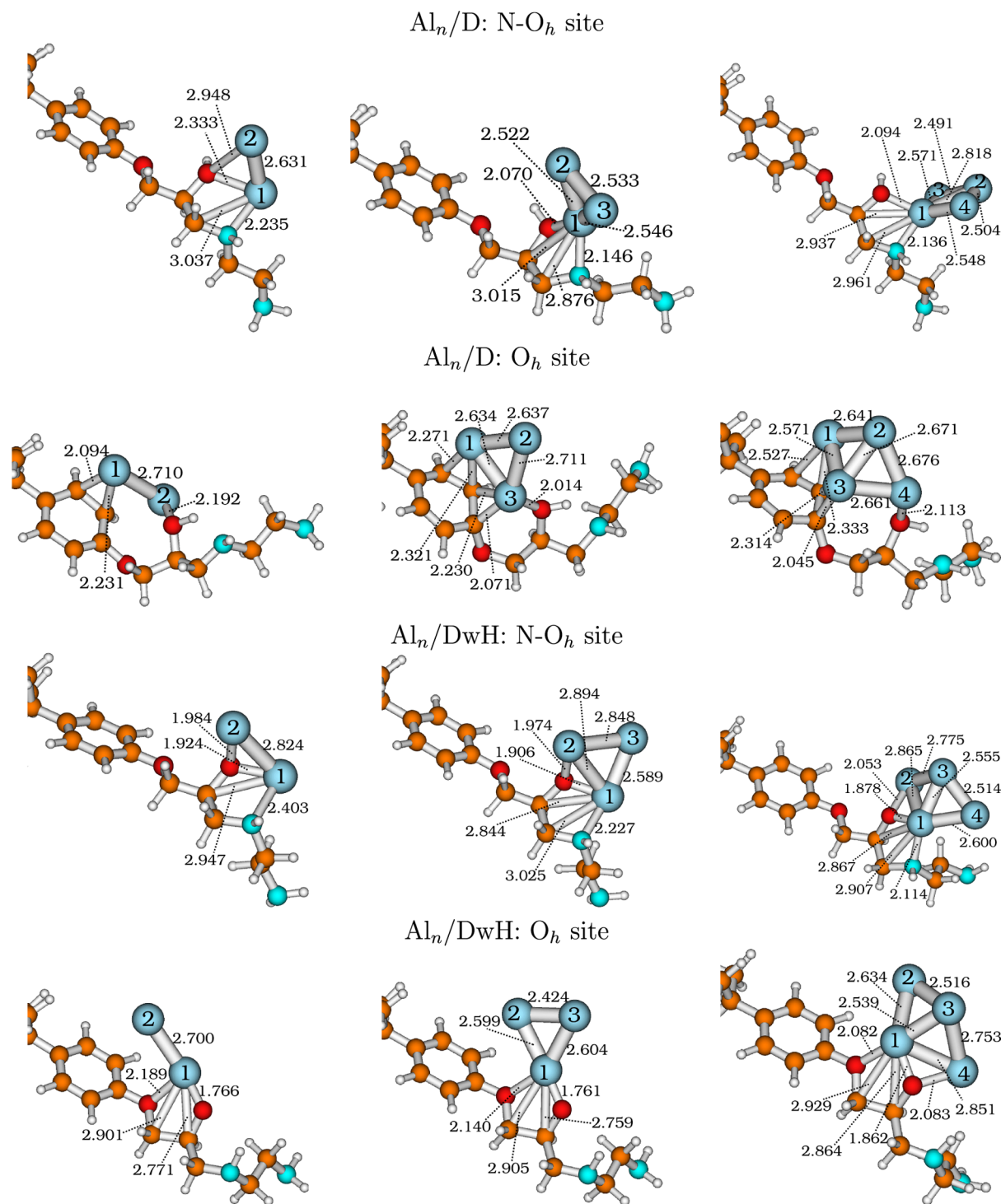
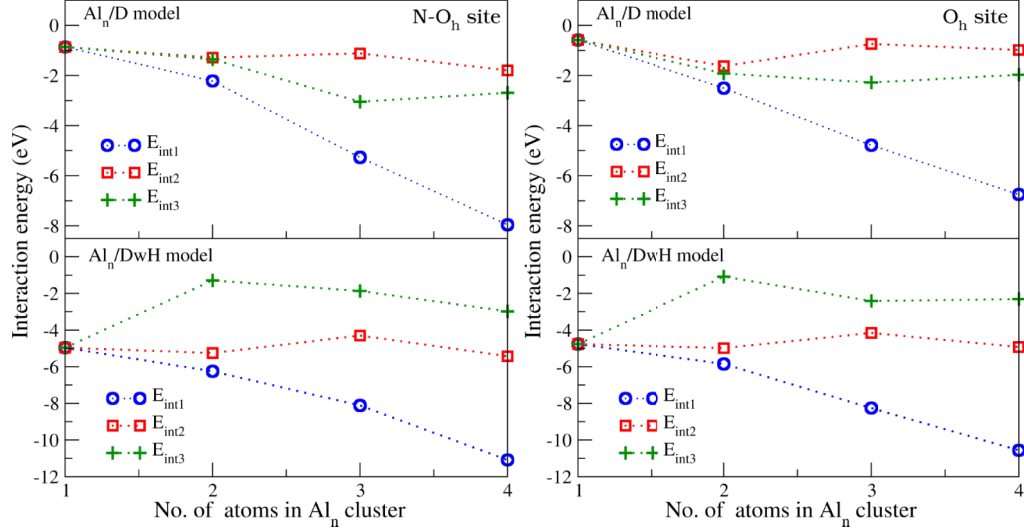


Figure 5. Most stable geometries (fully optimized) of the Al_n clusters adsorbed on D and DwH models at their N O_h and O_h sites, respectively. Bond lengths in Å.



		E_{int1}/n (eV/atom)			
		N- O_h		O_h	
n	Model	Al _n /D	Al _n /DwH	Al _n /D	Al _n /DwH
1		-0.865	-4.958	-0.585	-4.762
2		-1.109	-3.123	-1.251	-2.923
3		-1.755	-2.703	-1.593	-2.751
4		-1.989	-2.772	-1.687	-2.640

Figure 6. Interaction energies for simulated atom by atom deposition at the N O_h site (left) and O_h site (right), using fully optimized geometries of considered Al_n /substrate models.

In the following sections, we present an evolution of metal–organic interaction on increasing the number of Al atoms at the model interface as well as the impact on charge transfer at the interface.

3.3.2. Interaction Energy: Al_n /D or DwH Models. We present in Figure 5 the most stable Al_n /D or DwH structures ($n = 2–4$) for both N O_h and O_h sites, fully optimized using PBE D3/def2TZVP. In Al_n clusters, the nearest neighbor distances as well as their distances with substrate atoms at N O_h and O_h adsorption sites are also depicted in Figure 5. The average distances are 2.705 and 2.728 Å in Al_2 at N O_h and O_h sites, respectively, of Al_n /substrate models. In theoretical studies dedicated to Al_n clusters (refs^{72,73}), the bond length of Al_2 dimer is found to be 2.860 Å (exp. value = 2.700 Å⁷⁴) with a BE of 0.716 eV/atom. For Al_3 clusters at the N O_h (or at O_h) site, the avg. nearest neighbor distances are 2.534 (2.661) and 2.777 (2.542) Å corresponding to Al_3 /D and Al_3 /DwH models, respectively. In our case, Al_3 clusters are either nearly isosceles or equilateral triangles, as reported in previous works^{72,73,75} with an avg. nearest neighbor distance of ~ 2.61 Å. The stable Al_4 clusters are usually described as nearly rhombus or parallelogram^{72,75} with each side equal to (2.520–2.720) Å. We find distorted parallelograms (avg. edge value $\in \{2.529–2.689\}$ Å) for Al_4 clusters as their geometries are quite influenced by the presence of the substrate dimer. In this work, we are mainly interested in understanding the metal cluster interaction with polymeric substrates.

There are several possible ways to define interaction energy between the metal cluster Al_n and the polymeric substrate (D and DwH) representations. In eq 4, Interaction energy (E_{int1}) defines interaction of isolated Al atoms (present ensemble) on the substrate, considering Al–Al interaction, but without defining Al atoms as a single entity (or a group).

$$E_{int1} = E_{Al_n/substrate}^{tot} - E_{substrate}^{tot} - n \times E_{1Atom}^{tot} \quad (4)$$

where $E_{Al_n/substrate}^{tot}$ is the total energy of the system consisting of n Al atoms on the dimer (D or DwH) model.

The other definition for interaction energy (E_{int2}) can be

$$E_{int2} = E_{Al_n/substrate}^{tot} - E_{Al_n}^{tot} - E_{substrate}^{tot} \quad (5)$$

where $E_{Al_n}^{tot}$ is total energy of the isolated Al_n cluster in vacuum with fixed geometry, obtained when adsorbed on D or DwH model (SP calculation).

E_{int2} interaction energy supposes the group of Al atoms as one entity (or Al_n cluster), and therefore, it can also be written as $E_{int2} = E_{int1} - \Delta H_f^{Al_n}$, where $\Delta H_f^{Al_n}$ is enthalpy of formation of Al_n species in vacuum. To calculate $\Delta H_f^{Al_n}$, we consider frozen cluster geometries (imposed by the dimer) in vacuum (Table S4). These two definitions of interaction energy take the total energy ($E_{substrate}^{tot}$) of pristine dimer (D or DwH) as the reference value.

The formalism of E_{int3} is driven by the atom by atom deposition, where each time the reference system ($Al_{n-1}/$

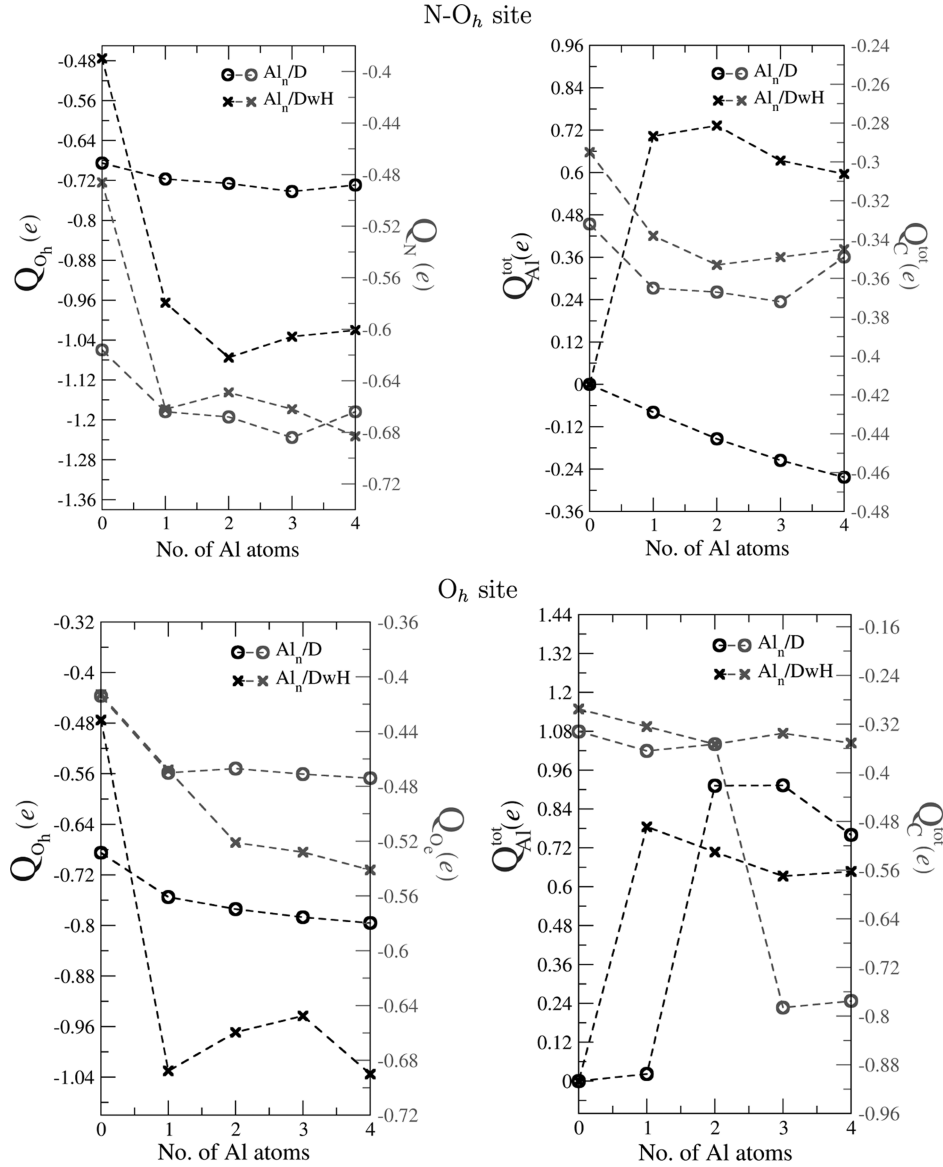


Figure 7. NBO charges (e) for simulated atom by atom deposition at N O_h and at O_h sites of the D and DwH models.

substrate) precedes the current system (Al_n /substrate). Thus, it represents evolution of interaction energy at the Al/epoxy interface.

$$E_{\text{int}3} = E_{Al_n/\text{substrate}}^{\text{tot}} - E_{Al_{n-1}/\text{substrate}}^{\text{tot}} - E_{1Al\text{atom}}^{\text{tot}} \quad (6)$$

where $E_{Al_n/\text{substrate}}^{\text{tot}}$ and $E_{Al_{n-1}/\text{substrate}}^{\text{tot}}$ are total energies of n and $(n - 1)$ atoms of aluminum adsorbed on the substrate (D or DwH) model, respectively.

The results of interaction energy calculations are presented in Figure 6 corresponding to both N O_h and O_h sites of the considered models, that is, Al_n /D and Al_n /DwH, where $n \in \{1-4\}$. The interfacial interaction between Al atoms and substrate models at N O_h and O_h sites of the substrate is evaluated. This provides insights into local chemical interaction of metal with two highly electronegative atoms (O, N), also, known to bond strongly with aluminum. Globally, we observe increase in strength of interaction on adding more Al atoms with respect to one Al atom on the substrate (D or DwH) structures, as indicated by $E_{\text{int}1}$ (blue open circles) values. It is expected because metal-metal interactions are

strong in comparison to metal-organic exchanges^{8,16} and favors the stability of the system. This trend is relevant to the two sites, one representing a hetero environment (N O_h) while the other (O_h) demonstrates interactions with mainly oxygen atoms. However, $E_{\text{int}1}/n$ values show contrasting behavior between Al_n /D and Al_n /DwH models. It is evident that adding more Al atoms on the D model increases the binding strength per atom ($E_{\text{int}1}/n$), while there is an almost reverse trend for adsorption on the DwH model. It illustrates that the dehydrogenation process accelerates the interaction mechanism to a saturation value per atom which decreases upon adding of more atoms. We observe a much flatter energy ($E_{\text{int}2}$ red open squares) evolution in terms of size of clusters than the former case. Clearly, the interaction energy at the N O_h site for Al_n /DwH models is much stronger ($E_{\text{int}2}$ range up to -5.4 eV approx.) than for Al_n /D models ($E_{\text{int}2}$ range up to -1.8 eV). Similarly, at the O_h site, $E_{\text{int}2}$ values vary up to -4.9 eV approx. and -1.5 eV approx. for Al_n /DwH and Al_n /D models, respectively. Thus, energetically, N O_h still remains the preferred interaction site for the formation of the Al/epoxy interface. Further, we can infer from $E_{\text{int}2}$ values that pairing

Table 3. Calculated BE Shifts Using Δ KS Theory for Models Shown in Figure 8^a

N-O _h site functional group	Al/DwH Δ BE (eV)	Al ₂ /DwH Δ BE (eV)	O _h site functional group	Al/DwH Δ BE (eV)	Al ₂ /DwH Δ BE (eV)
C _{ph} * C _q	0.08	0.00	C _{ph} * C _q	0.00	0.16
C _{ph}	0.04	0.00	C _{ph}	0.00	0.00
C _{ph}	0.07	0.08	C _{ph}	0.06	0.14
C _{ph}	0.12	0.11	C _{ph}	0.07	0.34
C _{ph}	0.19	0.32	C _{ph}	0.26	0.46
CH ₃	0.41	0.71	CH ₃	0.27	0.56
CH ₃	0.42	0.73	CH ₃	0.27	0.57
C _q	0.86	1.18	C _q	0.75	1.05
C _{ph} * O _e CH ₂ C(O Al)	1.68	1.84	C*H ₂ NH	0.91	1.13
C* O Al	2.03	2.66	C(O Al) C* NHC	0.97	1.24
C(O Al) C* NAIHC	2.07	2.60	C* O Al	1.53	1.76
C _{ph} O _e C*H ₂ C(O Al)	2.08	2.60	C _{ph} * (O _e Al) CH ₂ C(O Al)	1.74	1.93
C*H ₂ NAIH	2.19	2.30	C _{ph} (O _e Al) C*H ₂ C(O Al)	2.06	2.39

^aThe quaternary C atom is labeled as C_q, while C atoms in the phenyl ring is labeled as C_{ph}.

(or adhesion) between Al atoms as the dimer is favored at both sites of Al_{*n*}/D and Al_{*n*}/DwH models. Previous theoretical works^{29,66,76} on the Al/polymer interface preferred only Al dimer adsorption on simple polymeric models. On considering atom by atom deposition, the evolution of interaction energy is gauged with respect to a system (Al_{*n-1*}/substrate; *n* ∈ {2–4}) already in interaction with metal atoms. The *E*_{int3} values (green crosses) show difference in behavior of dimer (D and DwH) models on a gradual coverage by Al atoms. For the Al_{*n*}/D system, where *n* ∈ {2–4}, the interaction increases with respect to the Al/D model, like the presence of one Al atom facilitates further evolution at the interface. The *E*_{int3} values range up to –2.7 and –1.9 eV approx. at N O_h and O_h sites of Al_{*n*}/D models. The Al/DwH model illustrates the maximum interaction as the reactivity at its interface is facilitated by the dehydrogenation. However, further addition of Al atoms reduces the interaction energy (*E*_{int3}) to –3.0 and –2.3 eV approx. at N O_h and O_h sites of Al_{*n*}/DwH models, respectively. It is in accordance with explanation using *E*_{int1}/*n* values.

It can be deduced from this interaction energy analysis that Al_{*n*}/DwH models represent a higher interaction of Al atoms with the epoxy substrate than Al_{*n*}/D models. However, with more number of aluminum atoms (>4), the interaction mechanism (*E*_{int1}/*n* and *E*_{int3}) represented by Al_{*n*}/DwH and Al_{*n*}/D models might be similar. All interaction energy values are also provided (Table S3) in [Supporting Information](#).

3.3.3. Charge Transfer at the Interface. Our study reveals charge transfer at the Al/polymer interface to be mostly local, restricted to second neighbors of adsorbed Al atoms. The results of charge analysis using the NBO method are presented in [Figure 7](#) for fully optimized Al_{*n*}/substrate models ([Figure 5](#)) at N O_h (upper panel) and O_h sites (lower panel), respectively.

We show in [Figure 7](#) (upper left) net charges (*Q*) on N and O (belonging to hydroxy group) atoms and in [Figure 7](#) (upper right) the net total of charges (*Q*^{tot}) on Al atoms and C atoms as a function of number of Al atoms at the interface. At the O_h site of Al_{*n*}/substrate models, the *Q* on oxygen atoms (belonging to hydroxy and ether groups) are depicted in [Figure 7](#) (lower left) and *Q*^{tot} on Al atoms and C atoms are shown in [Figure 7](#) (lower right), with respect to number of Al atoms. The *Q*^{tot} represented for C atoms is obtained by adding charges on five carbon atoms (ID: 7, 10, 11, 12, and 13), that is, the ones directly bonded to either of O_e, O_h, or N atoms ([Figure 1](#)).

Mostly, charge transfer at the interface illustrated by Al_{*n*}/substrate models is aligned with electronegativities of atoms. The *Q*^{tot} carried by Al atoms is up to 0.65 e for Al_{*n*}/DwH models on an average at the N O_h site which suggests charge transfer toward N and O_h atoms. However, in Al_{*n*}/D models at this site, a slight negative average *Q*^{tot} (–0.18 e) is noted. NBO charges carried by the O_h atom increase from –0.68 e and –0.47 e for the pristine D and DwH models, respectively, to –0.73 e and –1.02 e for Al covered dimer models at the N O_h site. Also, for the N atom, negative charge gain is significant (–0.20 e) in the case of the Al_{*n*}/DwH system rather than the Al_{*n*}/D model. At the N O_h site, C atoms gain on average charge up to –0.06 e and –0.03 e on aluminum deposition with respect to D and DwH models, respectively.

At the O_h site of Al_{*n*}/substrate models, the charge transfer is slightly delocalized. The average *Q*^{tot} carried by Al atoms is 0.65 e and 0.69 e for Al_{*n*}/D and Al_{*n*}/DwH models, respectively. In Al_{*n*}/D models, average *Q* gained by O_h and O_e atoms is –0.09 e and –0.06 e, respectively. While average *Q*^{tot} gained by C atoms is –0.24 e because of the strong interaction of Al_{*n*} with C_{phenyl} at the O_h site of Al_{*n*}/D models. For Al_{*n*}/DwH models at this site, average charge gained by O_h, O_e, and N atoms is –0.56 e, –0.08 e, and –0.10 e, respectively. Also, average *Q*^{tot} gained by C atoms is –0.04 e for Al_{*n*}/DwH models. Globally, previous works on Al/PET,^{29,66} Al/PI,⁵⁶ and Al/polycaprolactone⁶⁶ elucidate the charge transfer from Al atoms acquiring a positive charge (avg. *Q*^{tot} ~ 1.00 e) mainly toward oxygen containing groups followed by ester carbons and C_{phenyl}. Aliphatic carbons usually acquire maximum charge up to –0.06 e. It is also shown that the negative charge gained by the polymeric substrate atoms leads to a shift toward lower BE values in the XPS spectrum. In this work, charge transfer at the interface represented by Al_{*n*}/DwH models fairly agrees with previous results on the Al/polymer interface.

3.4. Simulated XPS: Al/Poly-Epoxy Interface. The adsorption studies and the charge analysis indicate high probability of Al adsorption along with dehydrogenation at the surface. Also, among the possible interactions between Al and polymeric surface, the preferred one or the first site to be hosting Al atom(s) at the polymer surface is the O_h site. We present results of XPS simulations for both favorable and unfavorable possible scenarios pertaining to Al adsorption on substrate (D or DwH) models. Results of BE (or chemical) shifts for C 1s spectra of considered Al/poly epoxy models,

Table 4. Calculated BE Shifts Using Δ KS Theory for Models Shown in Figure 9

N-O _h site			O _h site		
functional group	Al/D	Al ₂ /D	functional group	Al/D	Al ₂ /D
	Δ BE (eV)	Δ BE (eV)		Δ BE (eV)	Δ BE (eV)
C _{ph}	0.00	0.00	C _{ph}	0.00	0.00
C _{ph}	0.11	0.07	C _{ph} Al	0.14	0.26
C _{ph} [*] C _q	0.16	0.10	C _{ph} Al	0.22	0.42
C _{ph}	0.17	0.14	C _{ph} [*] C _q	0.20	0.43
C _{ph}	0.39	0.39	C _{ph}	0.53	0.55
CH ₃	1.31	0.93	CH ₃	1.06	0.91
CH ₃	1.35	0.95	CH ₃	1.06	1.13
C _q	1.53	1.46	C _q	1.51	1.53
C _{ph} [*] O _e CH ₂ C(OH Al)	1.97	1.89	C _{ph} [*] O _e CH ₂ C(OH Al)	2.00	2.23
C [*] H ₂ NH(Al)	2.36	2.36	C [*] H ₂ NH	2.55	3.20
C(OH) C [*] N(Al)HC	2.97	2.80	C(OH Al) C [*] NHC	3.18	3.72
C _{ph} O _e C [*] H ₂ C(OH Al)	3.39	3.20	C _{ph} O _e C [*] H ₂ C(OH Al)	3.44	3.93
C [*] OH Al	3.50	3.00	C [*] OH Al	3.43	3.82

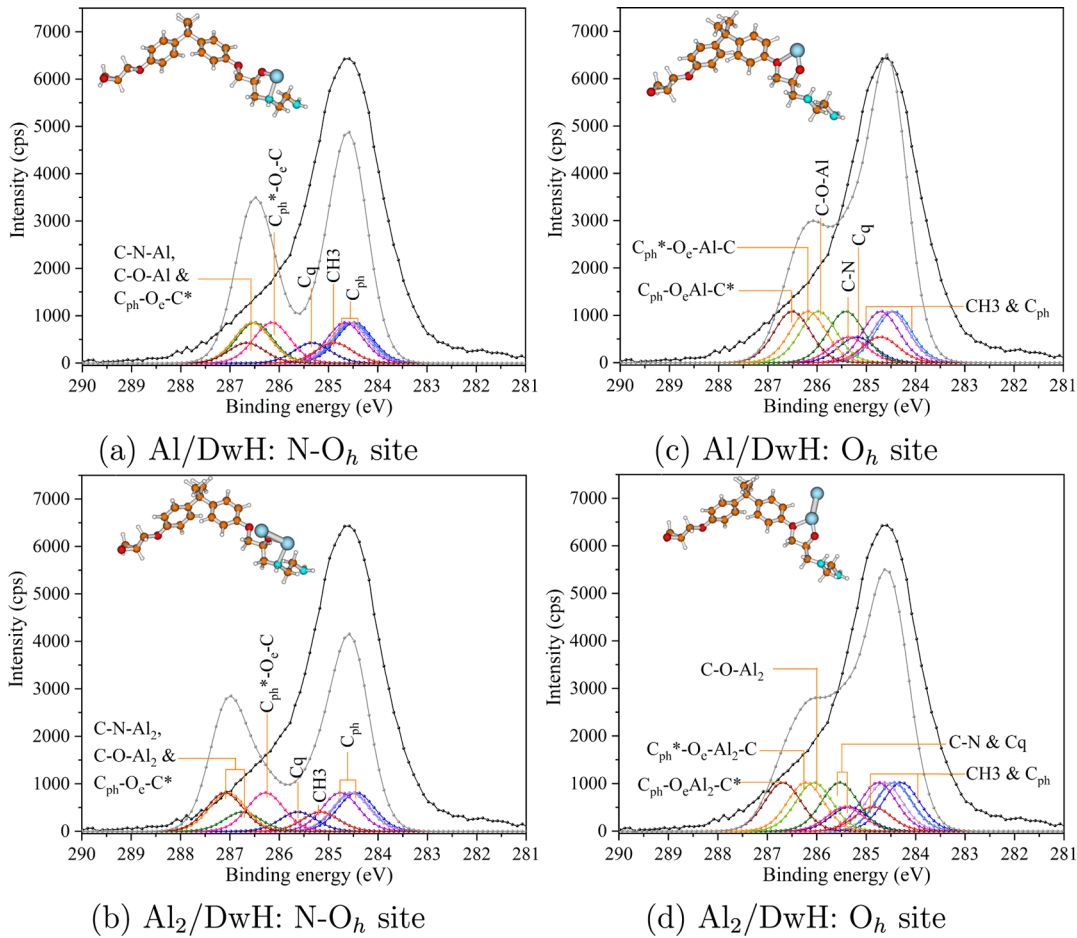


Figure 8. Experimental C 1s spectrum (in black) for the Al/poly epoxy buried interface. XPS simulations using Δ KS theory for (a,c) Al/DwH and (b,d) Al₂/DwH models at the N O_h and O_h sites. Simulated spectra are shown in gray. Adsorbed Al atom(s) is depicted as blue sphere(s).

using the Δ KS method, are summarized in Tables 3 and 4. These values are then employed to construct simulated C 1s spectra with a fwhm (full width at half maximum) value equal to 0.9 eV and a stoichiometry ratio corresponding to 2DGEB/1EDA (fixed relative areas). We present the decomposition of experimental C 1s using Al₍₂₎/DwH models for the N O_h site in Figure 8a,b and for the O_h site in Figure 8c,d, respectively. Similarly, simulated C 1s XPS spectra using Al₍₂₎/D models are shown in Figure 9 for both N O_h and O_h sites.

In all cases, the black curves exhibit the shape of experimental C 1s of the buried interface observed after 110 s of Ar⁺ etching. The gray envelopes represent the simulated spectra obtained by summing over all components of chemical shifts calculated for each representative model (see Figures 8 and 9). Experimentally, we examine that a C 1s shoulder peak is present at 286.3 eV for the pristine surface (Figure 2), while on metal adsorption, this shoulder peak disappears. As explained in [refs^{20,57}], the reason is chemical shift toward lower BEs, moving from pristine C–O contributions to the

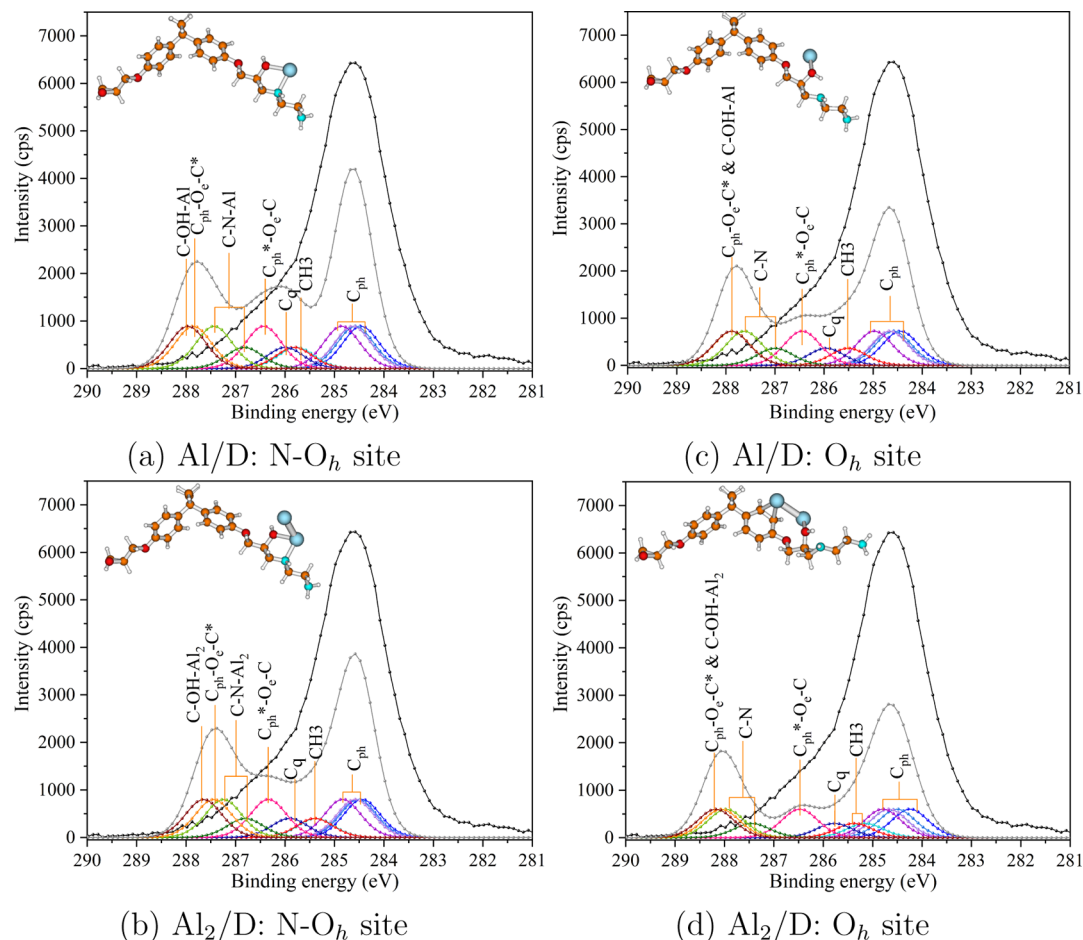


Figure 9. C 1s spectrum (in black) for the Al/poly epoxy buried interface. XPS simulations using Δ KS theory for (a,c) Al/D and (b,d) Al₂/D models at N O_h and O_h sites. Simulated envelopes are presented in gray color. Adsorbed Al atoms are shown as blue spheres.

metal adsorbed surface with contribution from C–O–M (M = metal) formations. In the present study, the formation of C–O–Al bonds is also favorable and corresponds well with experiments when their calculated Δ BE is small compared to the Δ BE(C–OH) contribution present in the pristine surface (see Table S1). These chemical shifts toward lower BE in (N,O) containing polymers can vary depending on the available reactive sites at the surface, comparative bond strength of reactive functional groups,^{24,58} diffusion tendency of metals,^{18,57} and nature of charge transfer at the interface.^{29,77,78} Through XPS analysis in Figures 8 and 9, we assess the effect of two different chemical environments (N O_h or O_e–O_h site), changes with respect to metal–metal bonding and positive influence of dehydrogenation on Al adsorption. The simulated C 1s spectra of Al₍₂₎/DwH models exhibiting Al–N interaction do not correspond well to the experimental C 1s spectrum (Figure 8) because N–H (present in considered dimer models) does not exist in the real cross linked polymer. An increase in high BE shoulder (around 286.3 eV) is depicted by simulations, mainly because C–N contributions from chemisorption of Al₍₂₎ at the N O_h site of the DwH model. A fair correspondence with the experimental spectrum can be drawn using Al₍₂₎/DwH models at the O_h site. The calculated values of chemical shifts for C atoms belonging to various functional groups (Table 3) lead to a reasonable decomposition of experimental C 1s spectra. We note a

significant shift of 0.96 and 0.61 eV to low BE values (w.r.t. pristine model) for C–N and C–O contributions, respectively.

Al₍₂₎/D models show divergence in chemical shifts for all components for both N O_h and O_e–O_h environments, removing the distinct presence of a high intensity peak at 284.6 eV (Figure 9). Another observation for the Al_n/D system is that for $n = 4$, convergence in BE shifts is noticeable and C 1s peaks for both considered sites are similar. This is because of the increase in reactivity or charge transfer to carbon atoms via oxygen or nitrogen atoms on increasing the flux of Al atoms. Moreover, we observe a homogenizing effect for Al interaction at N O_h and O_h sites for $n(\text{Al}) = 4$, given the limited size of our model system (see Figure S7 and Table S13). Overall, Al₍₂₎/DwH models appear as a fair representation of the Al/epoxy interface because the reactivity with metal atoms is promoted by the dehydrogenation process. However, our study indicates that similar results with Al_n/D models might be achievable by increasing $n(\text{Al})$ at the interface.

4. DISCUSSION

4.1. Reactivity Modification at N Site. Comparative XPS analysis point toward metal adsorption at the N O_h site to be the least probable during initial stages of metallic layer growth on poly epoxy surfaces. It is expected because the secondary amine (–NH) group present in the representative dimer model does not exist in real epoxy polymers. Also, sp³ nitrogen connected to a hydrogen is more reactive than the one bonded

only to carbon atoms. Thus, to verify limitations of the substrate (dimer) models and the validity of our adsorption/interaction study, we replaced H atom (attached to N) by a $-\text{CH}_3$ (methyl) group. In Figure 10, we present these optimized geometries, namely, $\text{Al}/\text{D}^{(\text{N}-\text{CH}_3)}$ and $\text{Al}/\text{DwH}^{(\text{N}-\text{CH}_3)}$ models showing the adsorption at the two stable sites.

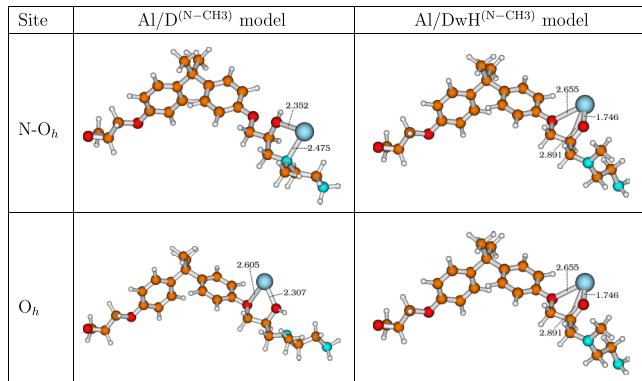


Figure 10. $\text{Al}/\text{D}^{(\text{N}-\text{CH}_3)}$ and $\text{Al}/\text{DwH}^{(\text{N}-\text{CH}_3)}$ models for Al atom adsorption at N O_h and O_h sites. Bond distances are in Å, PBE D3/def2TZVP level of theory.

The results regarding this chemical environment modification at the N site are shown in Table 5. The N O_h site remains

Table 5. Interaction and Adsorption Energies (in eV) and NBO Charges (in e) on the Al Atom for $\text{Al}/\text{D}^{(\text{N}-\text{CH}_3)}$ and $\text{Al}/\text{DwH}^{(\text{N}-\text{CH}_3)}$ Models Using PBE D3/def2TZVP Level of Theory

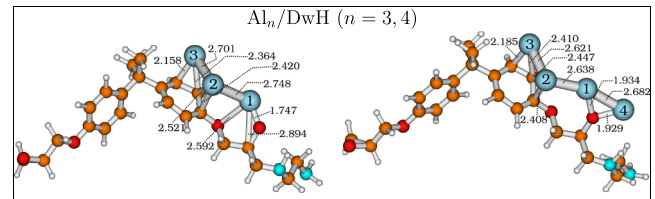
	site	E_{int}	E_{ads}	Q_{Al}
$\text{Al}/\text{D}^{(\text{N}-\text{CH}_3)}$	N O_h	0.767	0.767	+0.43
	O_h	0.586	0.586	+0.02
$\text{Al}/\text{DwH}^{(\text{N}-\text{CH}_3)}$	N O_h	4.776	2.795	+0.72
	O_h	4.505	2.524	+0.78

energetically more favorable than the O_h site for aluminum adsorption even after the removal of secondary amine. Overall, adsorption energies indicate physisorption on the dimer ($\text{D}^{(\text{N}-\text{CH}_3)}$) model at the O_h site and chemisorption on the dehydrogenated ($\text{DwH}^{(\text{N}-\text{CH}_3)}$) model for both sites. In the case of the $\text{D}^{(\text{N}-\text{CH}_3)}$ model, because of the presence of H ($-\text{OH}$ group), the impact on reactivity (interaction/adsorption) stays localized to the N atom. On comparison with Al/D (N O_h site), Al-N bond distance changes from 2.361 to 2.475 Å for the $\text{Al}/\text{D}^{(\text{N}-\text{CH}_3)}$ model. For other near neighbors to the Al atom, the distances change up to 0.02 Å irrespective of the site. It can be a reason for no change in adsorption energy at the O_h site, while $|E_{\text{ads}}|$ decreases by 98 meV at the N O_h site compared to Al/D models. Also, no change in charge on the Al atom is observed at the O_h site, while the charge on the Al atom (+0.43 e) at the N O_h site notably changes on comparison with Al/D models.

$\text{Al}/\text{DwH}^{(\text{N}-\text{CH}_3)}$ models also indicate a decrease in interaction or adsorption, which corresponds well with the N site becoming less reactive on replacing H by the $-\text{CH}_3$ group. We observe decrease in $|E_{\text{int}}|$ values by 200 meV approx. for both considered sites. The values of adsorption energies remain same at the N O_h site, while $|E_{\text{ads}}|$ decreases at the O_h

site by 75 meV approx. Also, near neighbor bond distances for adsorbed Al atom on $\text{DwH}^{(\text{N}-\text{CH}_3)}$ only change up to 0.018 Å at maximum with respect to DwH models, independent of the site. For the $\text{D}^{(\text{N}-\text{CH}_3)}$ model, $E_{\text{diss}}^{\text{OH}}$ is equal to 4.248 eV. This value is sensitive to a slight change in molecule geometry and modified by 181 meV with respect to the D model. It can be concluded that removal of secondary amine does not affect the energetic order of adsorption sites. Hence, the representative picture of chemical behavior at the Al/epoxy interface remains the same.

4.2. Linear Versus Cluster Configuration. Combined experimental and theoretical XPS results suggest $\text{Al}_{(2)}/\text{DwH}$ models at the O_h site to be a fair representation of the Al/poly epoxy interface. To further understand how the metallization proceeds in the low coverage regime, we have simulated both linear and cluster type growth scenarios. The linear (1D) configurations for Al_n/DwH ($n = 3, 4$; O_h site) are shown in Figure 11 along with tabulated interaction energies. Energeti



	Linear configurations at O_h site			
	E_{int1} (eV)	E_{int2} (eV)	E_{int3} (eV)	E_{int1}/n (eV/atom)
Al_3/DwH	-7.803	-4.740	-1.957	-2.601
Al_4/DwH	-9.520	-4.935	-1.266	-2.380

Figure 11. Al_n/DwH models for aluminum adsorption at the O_h site in open chain like configuration. Bond distances are in Å. Interaction energies are assembled in tabulated form, PBE D3/def2TZVP level of theory.

cally, the 1D arrangement of Al atoms (Figure 11) is less favorable than nearly 2D (flat) cluster arrangement (Figure 5) for the Al_n/DwH ($n = 3, 4$; O_h site) system.

Further in detail, we observe that the interaction per Al atom ($|E_{\text{int1}}/n|$) decreases up to 260 meV with respect to the cluster arrangement. Also, $|E_{\text{int3}}|$ values decrease up to 1000 meV implying that atom by atom deposition is less stable in a linear arrangement compared to 2D/3D arrangement of Al atoms at the interface with epoxies. On comparing $|E_{\text{int2}}|$ values, which account for the group of Al atoms as one entity, the interaction increases by 590 and 14 meV for the Al trimer and tetramer, respectively, in the Al_n/DwH ($n = 3, 4$; O_h site) system. It is because of decrease in $|\Delta H_f^{\text{Al}}|$ values of isolated (in vacuum) linearly arranged Al trimer or tetramer compared to their nearly planar forms. However, the disparity observed in $|E_{\text{int2}}|$ values could exhibit that at a higher flux of metal deposition, only layer by layer growth fashion could be envisaged on poly epoxy surfaces. In ref 18 using *in situ* XPS, for thickness of Al layers up to 2.1 nm on the epoxy resin surface, chemisorption tendency of Al with layer by layer growth is proposed. In contrast, bounded by the size of our model epoxy system, our calculations suggest arrangement of Al atoms in a nearly planar (2D/3D) cluster form at the very initial stage (below 1 nm) of Al/epoxy interface formation.

4.3. Electronic Structure. From the point of view of the electronic structure, usually the charge transfer in metal/organic interfaces is described as a two fold process. Charge is

usually transferred from the occupied MO of the isolated metal system to an unoccupied orbital of the organic system. This process is sometimes followed by a second process, leading to back donation of charge from the organic system to the metal.^{29,66,76} We present in [Figure 12](#) density of states (DOS)

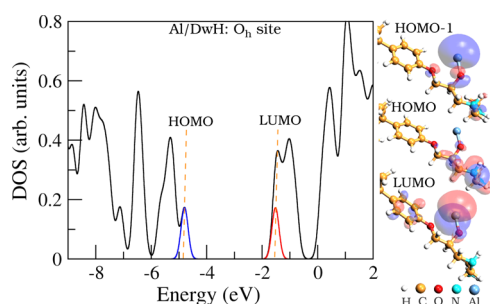


Figure 12. Total DOS of Al/DwH model (a restricted closed shell system) at the O_h site are presented in black. The isosurface HOMO–LUMO representations plotted at an isovalue of $0.03 \text{ e}/\text{\AA}^3$; color code for isosurface values is positive = blue and negative = red.

of the Al/DwH model at the O_h site. It highlights the impact of aluminum adsorption on the electronic structure of the pristine model epoxy system (see [Figure S8](#)). Also, the Al/DwH model (at O_h site), among all considered model systems, exhibits the best correspondence with experiments which makes it interesting to study from the perspective of electronic structure properties. Here, the DOS spectrum is constructed as a sum of Gaussian functions centered at discrete positions of energy levels (not shown) with fwhm equal to 0.5 eV.⁷⁹ The position of the highest occupied MO (HOMO) level is indicated by the blue curve, and all states below it are occupied states. However, the lowest unoccupied MO (LUMO) level position is represented by red curve and all states above it are unoccupied. On Al adsorption, occupied states appearing in the HOMO–LUMO gap (E_g) present in pristine dimer ([Figure S8](#)) leading to narrowing of its width. The E_g value is 3.83 eV for pristine dimer (D) and it decreases to 3.28 eV for the Al/DwH system (see [Table S14](#)). Increase in intensities of peaks at low energies can be observed after chemisorption of Al atom(s) ([Figures S12](#) and [S8](#), lower panel) on comparison with DOS of the pristine dimer ([Figure S8](#), upper panel). This is a result of filling of LUMO levels of molecular systems, which in turn stabilizes them close to their HOMO levels.

Monitoring the changes of interfacial chemistry before and after metal adsorption in the DOS spectra of highly interacting systems is not trivial as suggested in [ref 76](#) about the aluminum/polythiophene interface. Interestingly, the analysis of the frontier MOs also provides insight into the charge transfer in a metal/organic interface owing to their electronic structure. Localization of LUMO levels of the isolated molecular system is crucial to understand their interaction with occupied levels of the isolated metal system during adsorption. The LUMO of the D model has mainly π character and is localized to phenyl rings, while the LUMO of the DwH is primarily localized at the cured part of the epoxy molecule, which is a more realistic chemical representation of poly epoxies (see [Figure S8](#) upper panel). Detailed description of HOMO–LUMO isosurface plots of D and DwH models is provided in [Supporting Information](#).

In [Figure 12](#), the isosurface plot of the HOMO – 1 level of Al/DwH (a restricted closed shell) system is localized over the

aluminum atom with large atomic orbital (AO) contributions, that is, Al (s, p_y, p_z, dx^2). Other major contributions include C_{phenyl} (s, p_y, p_z), O_e (s, p_y, p_z), and O_h (s, p_x, p_y, p_z). This strong presence of AO from the Al atom indicates the charge transfer from an occupied level of the Al atom to LUMO levels of the isolated DwH model, which thereby stabilizes as the HOMO – 1 of the Al/DwH system. Also, the HOMO level of the Al/DwH system is mainly localized over the cured part of model epoxy, that is, $O_h, C^*–O_h$ and N atoms. Depopulation of occupied levels of Al atoms on interaction with model epoxy also leads to substantial AO contributions from the Al atom to the LUMO level of the Al/DwH system. Also, this level has π character localized over the phenyl ring. Localization of HOMO–LUMO isosurfaces further outlines the charge transfer from the aluminum atom to model epoxy in the Al/DwH system at the O_h site.

4.4. Consideration of Oxidation in Molecular Models.

The experimental XPS study in this work is based on the buried interface accessed by etching the Al/epoxy sample and, hence, removing surface contamination and oxide layer formation. However, the presence of aluminum oxide layer is usually inevitable. Also, air exposed aluminum film leads to the possible presence of different surface species such as Al_2O_3 , $AlOOH$, and $Al(OH)_3$.^{62,80} To explore an aspect of surface oxidation, we consider simultaneous interaction of $Al(OH)_3$ and Al atom(s) with the DwH dimer model at the O_h site. The two stable fully optimized configurations determined in this quest, using PBE D3/def2TZVP level of theory, are shown in [Figure 13a](#): $Al–Al(OH)_3/DwH$ and [Figure 13b](#): $Al_3–Al(OH)_3/DwH$. The interaction of these metal–(metal hydroxide) with the DwH dimer is much stronger than only Al interaction with the polymeric substrate as evidenced by the interaction energy values. In this case, interaction can be described by modified version of [eq 5](#), that is, $E_{\text{int}} = E_{Al_n–Al(OH)_3/DwH}^{\text{tot}} - E_{Al_n–Al(OH)_3}^{\text{tot}} - E_{DwH}^{\text{tot}}$, where $n = 1$ or 3. The value $|E_{\text{int}}|$ for $Al–Al(OH)_3/DwH$ is 9.577 eV, that is, it exhibits more interaction in comparison to interaction illustrated by its parent model Al/DwH with $|E_{\text{int}}| = 4.763$ eV.

Similarly, $Al_3–Al(OH)_3/DwH$ with $|E_{\text{int}}| = 5.538$ eV implies stronger interaction of $Al_3–Al(OH)_3$ with the molecular model as to interaction in its nonoxidized version, that is, Al_3/DwH ($|E_{\text{int}}| = 4.149$ eV). Finally, we perform simulated XPS calculations using Δ KS theory for O 1s and Al 2p as presented in [Figure 13c,d](#), and [e,f](#), respectively, corresponding to $Al–Al(OH)_3/DwH$ and $Al_3–Al(OH)_3/DwH$ models. Consideration of oxidation effects as an extension to, so far, the most suitable molecular model: Al/DwH leads to fine decomposition of the experimental O 1s spectra. The asterisk (*) in the labels of functional groups marks the atom contributing to the Δ BE value. The O 1s spectrum (Al/poly epoxy) is symmetric with $Al–O^*H$ components (from the presence of $Al(OH)_3$) around low BE values (530.8 eV), $C–O^*Al–Al(OH)_3$ (from oxygen of the dimer with the simultaneous presence of metal and metal hydroxide) at 531.1 eV and $C_{\text{ph}}–O_e^*–C$ and $Al–O^*(H)–Al(OH)_2$ around 532 eV, respectively. After coverage of the Cu film on poly epoxy, the O 1s peak was observed to be rather broad and nonsymmetric.²⁰ We are able to simulate the oxide part of the Al 2p peak ([Figure 13e](#)) using the $Al–Al(OH)_3/DwH$ model. However, only from the $Al_3–Al(OH)_3/DwH$ model with the presence of Al atoms (numbered blue spheres) in both neutral and oxidized states (see Q_{Al} values in [Figure 13f](#)), we could simultaneously

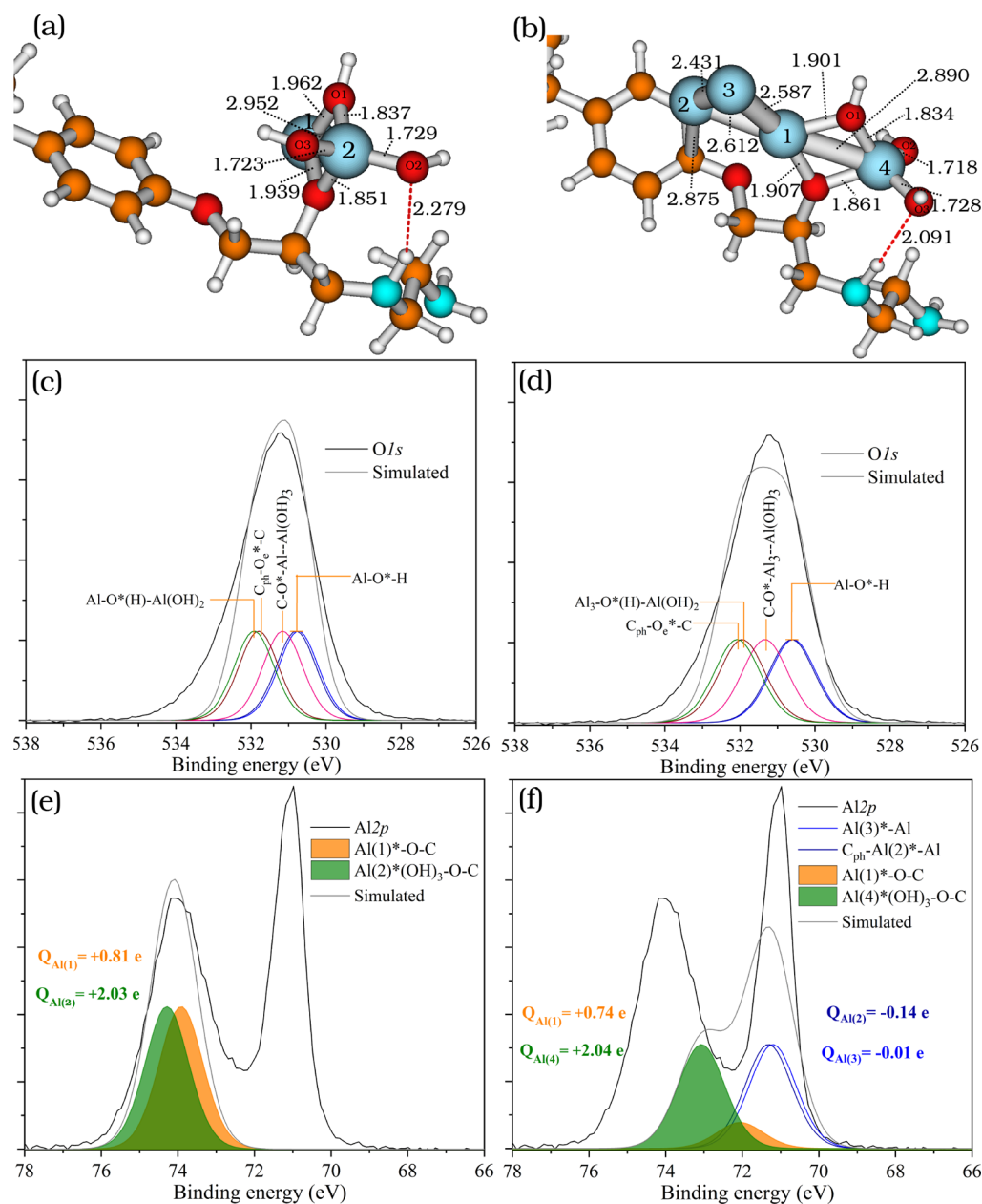


Figure 13. Optimized structures showing interactions at the O_h site between (a) Al–Al(OH)₃ and DwH dimer (b) Al₃–Al(OH)₃ and DwH dimer model, using PBE D3/def2TZVP level of theory. Bond distances are in Å. Experimental O 1s (c,d) and Al 2p (e,f) XPS spectra of the Al covered poly epoxy surface (black line) along with simulated spectra (gray line) obtained using Δ KS theory. Simulated XPS spectra in the left panel and right panel represent BEs calculated for molecular models in (a,b), respectively. NBO charges (in e) on Al atoms indexed 1 to 4 are provided in Al 2p (e,f) XPS spectra.

decompose metallic and oxidized parts of the Al 2p peak. Also, the C 1s spectra of the models accounting for surface oxidation are presented in Figure S8. The values of BE shifts calculated for C 1s, O 1s and Al 2p spectra are gathered in Table S15. Globally, consideration of the naturally occurring presence of Al surface hydroxide in the molecular models brings out a fair match with O 1s and Al 2p experimental spectra.

5. CONCLUSIONS

To conclude, using a molecular epoxy model, we perform a detailed study of metallization energetics. It helps to reveal physicochemical interplay at the Al/epoxy interface for very initial stage of metal deposition, limited to atomic scale. Our DFT calculations using all electron potentials indicate

chemisorption of aluminum on the DwH model. On the other hand, interaction energy calculations and charge transfer study delineate the change from physisorption to chemisorption on adding more atoms on the dimer (D) model at the O_h site. A comparative XPS study using the buried Al/poly epoxy interface clearly points to the Al/DwH model system at the O_h site to exhibit a fair correspondence between experiments and quantum chemical calculations. The presence of secondary amine in considered model systems does not affect the adsorption study. We discussed simulated atom by atom metal deposition using D and DwH model epoxy systems. Further, energetics of linear and 2D/3D configurations are compared using the Al_n/DwH system at the O_h site. Our study suggests the presence of nearly planar

aluminum clusters to be energetically favorable. The combined experimental and theoretical analyses highlight that the Al metal atoms starts chemical–covalent interaction with poly epoxy at the hydroxy group. Also, the initially deposited aluminum metal atoms act as nucleation sites for the formation of metallic islands or Al overlayers. Electronic structure properties (HOMO–LUMO isosurfaces) highlights the dehydrogenation of the poly epoxy surface to facilitate aluminum chemical adsorption. They also outline the charge transfer from Al atoms to the molecular (epoxy) system. Combination of XPS and AFM analyses reveals thickness of the Al film about 10 nm with the slight presence of the native oxide layer. An extension of the Al/DwH molecular model considering oxidation at the poly epoxy surface highlight a fair decomposition of O 1s and Al 2p experimental spectra. Overall, the approach adopted in this work can be broadly applied to understand and craft materials design strategies for systems dealing with metal–polymer interfaces.

■ ASSOCIATED CONTENT

● Supporting Information

The Supporting Information is available free of charge at <https://pubs.acs.org/doi/10.1021/acsami.0c19616>.

Pristine surface XPS (C 1s and O 1s), experimental XPS analysis after Al deposition (Al 2p and O 1s), simulated atom by atom deposition, charge difference after Al deposition with respect to the pristine surface, BE: relative stability of clusters, partial optimization at the N O_h site, and simulated C 1s using uGTS theory, and Al₄/D model: XPS, electronic structure properties, and consideration of surface oxidation (PDF)

■ AUTHOR INFORMATION

Corresponding Author

Kanika Anand – CIRIMAT, Université de Toulouse, CNRS INP ENSIACET, 31030 Toulouse Cedex 4, France; orcid.org/0000-0003-2054-3056; Email: kanika.anand@toulouse.inp.fr

Authors

Thomas Duguet – CIRIMAT, Université de Toulouse, CNRS INP ENSIACET, 31030 Toulouse Cedex 4, France; orcid.org/0000-0001-5432-2468

Jérôme Esvan – CIRIMAT, Université de Toulouse, CNRS INP ENSIACET, 31030 Toulouse Cedex 4, France

Corinne Lacaze Dufaure – CIRIMAT, Université de Toulouse, CNRS INP ENSIACET, 31030 Toulouse Cedex 4, France; orcid.org/0000-0003-3151-2685

Complete contact information is available at: <https://pubs.acs.org/doi/10.1021/acsami.0c19616>

Notes

The authors declare no competing financial interest.

■ ACKNOWLEDGMENTS

Authors are grateful to Cédric Charvillat for AFM measurements and technical support. We thank Maëllenn Aufray for fruitful discussions about polymerization of cured epoxies and Claire Tendero for thickness measurements on the epoxy substrate. We also acknowledge Diane Samelor for technical support. We thank CALMIP for HPC resources under the project p1526. Authors acknowledge the Agence Nationale de

la Recherche for funding of the OPOSUM project under project no. ANR 18 CE08 0010 01.

■ REFERENCES

- (1) Kubo, Y.; Tanaka, H.; Saito, Y.; Mizoguchi, A. Fabrication of a Bilayer Structure of Cu and Polyimide to Realize Circuit Micro miniaturization and High Interfacial Adhesion in Flexible Electronic Devices. *ACS Appl. Mater. Interfaces* **2018**, *10*, 44589–44602.
- (2) Yu, S.; Sun, Y.; Ni, Y.; Zhang, X.; Zhou, H. Controlled Formation of Surface Patterns in Metal Films Deposited on Elasticity Gradient PDMS Substrates. *ACS Appl. Mater. Interfaces* **2016**, *8*, 5706–5714.
- (3) Gensch, M.; Schwartzkopf, M.; Ohm, W.; Brett, C. J.; Pandit, P.; Vayalil, S. K.; Bießmann, L.; Kreuzer, L. P.; Drewes, J.; Polonskyi, O.; Strunskus, T.; Faupel, F.; Stierle, A.; Müller Buschbaum, P.; Roth, S. V. Correlating Nanostructure, Optical and Electronic Properties of Nanogranular Silver Layers During Polymer Template Assisted Sputter Deposition. *ACS Appl. Mater. Interfaces* **2019**, *11*, 29416–29426.
- (4) Duguet, T.; Senocq, F.; Laffont, L.; Vahlas, C. Metallization of Polymer Composites by Metalorganic Chemical Vapor Deposition of Cu: Surface Functionalization Driven Films Characteristics. *Surf. Coat. Technol.* **2013**, *230*, 254–259.
- (5) Lee, S.; Shin, S. J.; Baek, H.; Choi, Y.; Hyun, K.; Seo, M.; Kim, K.; Koh, D. Y.; Kim, H.; Choi, M. Dynamic Metal Polymer Interaction for the Design of Chemoselective and Long Lived Hydrogenation Catalysts. *Sci. Adv.* **2020**, *6*, No. eabb7369.
- (6) Capek, I. Polymer Decorated Gold Nanoparticles in Nano medicine Conjugates. *Adv. Colloid Interface Sci.* **2017**, *249*, 386–399.
- (7) Shi, J.; Votruba, A. R.; Farokhzad, O. C.; Langer, R. Nanotechnology in Drug Delivery and Tissue Engineering: From Discovery to Applications. *Nano letters* **2010**, *10*, 3223–3230.
- (8) Faupel, F.; Zaporozhchenko, V.; Strunskus, T.; Erichsen, J.; Dolgner, K.; Thran, A.; Kiene, M. *Metallization of Polymers 2*; Springer, 2002; pp 73–96.
- (9) Kim, D. H.; Jo, W. H. Studies on Polymer–Metal Interfaces. 2. Competitive Adsorption between Oxygen and Nitrogen Containing Functionality in Model Copolymers onto Metal Surfaces. *Macro molecules* **2000**, *33*, 3050–3058.
- (10) Kisin, S.; Božović Vukić, J.; van der Varst, P. G. T.; de With, G.; Koning, C. E. Estimating the Polymer–Metal Work of Adhesion from Molecular Dynamics Simulations. *Chem. Mater.* **2007**, *19*, 903–907.
- (11) Singh, B.; Hyun, J. Y.; Singh, A. P.; Gandhi, D.; Wu, Z.; Interrante, L. V.; Ramanath, G. Selective Deposition of a Cross Linked Low Permittivity Polycarbosilane on Copper. *ACS Appl. Mater. Interfaces* **2010**, *2*, 2180–2184.
- (12) Mohn, F.; Repp, J.; Gross, L.; Meyer, G.; Dyer, M. S.; Persson, M. Reversible Bond Formation in a Gold Atom–Organic Molecule Complex As a Molecular Switch. *Phys. Rev. Lett.* **2010**, *105*, 266102.
- (13) Valega Mackenzie, F. O.; Thijsse, B. J. Study of Metal/Epoxy Interfaces between Epoxy Precursors and Metal Surfaces Using a Newly Developed Reactive Force Field for Alumina Amine Adhesion. *J. Phys. Chem. C* **2015**, *119*, 4796–4804.
- (14) Bahlakeh, G.; Ramezanzadeh, B.; Saeb, M. R.; Terry, H.; Ghaffari, M. Corrosion Protection Properties and Interfacial Adhesion Mechanism of an Epoxy/polyamide Coating Applied on the Steel Surface Decorated with Cerium Oxide Nanofilm: Complementary Experimental, Molecular Dynamics (MD) and First Principle Quantum Mechanics (QM) Simulation Methods. *Appl. Surf. Sci.* **2017**, *419*, 650–669.
- (15) Ebadi, M.; Nasser, A.; Carboni, M.; Younesi, R.; Marchiori, C. F. N.; Brandell, D.; Araujo, C. M. Insights into the Li Metal/Organic Carbonate Interfacial Chemistry by Combined First Principles Theory and X Ray Photoelectron Spectroscopy. *J. Phys. Chem. C* **2019**, *123*, 347–355.
- (16) Nagy, G.; Walker, A. V. Dynamics of Reactive Metal Adsorption on Organic Thin Films. *J. Phys. Chem. C* **2007**, *111*, 8543–8556.

- (17) Thran, A.; Kiene, M.; Zaporajtchenko, V.; Faupel, F. Condensation Coefficients of Ag on Polymers. *Phys. Rev. Lett.* **1999**, *82*, 1903–1906.
- (18) Kanzow, J.; Horn, P. S.; Kirschmann, M.; Zaporajtchenko, V.; Dolgner, K.; Faupel, F.; Wehlack, C.; Possart, W. Formation of a Metal/epoxy Resin Interface. *Appl. Surf. Sci.* **2005**, *239*, 227–236.
- (19) Capricho, J. C.; Fox, B.; Hameed, N. Multifunctionality in Epoxy Resins. *Polym. Rev.* **2020**, *60*, 1–41.
- (20) Duguet, T.; Gavrielides, A.; Esvan, J.; Mineva, T.; Lacaze Dufaure, C. DFT Simulation of XPS Reveals Cu/Epoxy Polymer Interfacial Bonding. *J. Phys. Chem. C* **2019**, *123*, 30917–30925.
- (21) Sandrin, L.; Sacher, E. X Ray Photoelectron Spectroscopy Studies of the Evaporated Aluminum/Corona Treated Polyethylene Terephthalate Interface. *Appl. Surf. Sci.* **1998**, *135*, 339–349.
- (22) Friedrich, J. F.; Koprinarov, I.; Giebler, R.; Lippitz, A.; Unger, W. E. S. Reactions and Intermediates at the Metal Polymer Interface As Observed by XPS and NEXAFS Spectroscopy. *J. Adhes.* **1999**, *71*, 297–321.
- (23) Wolany, D.; Fladung, T.; Duda, L.; Lee, J. W.; Gantenfort, T.; Wiedmann, L.; Benninghoven, A. Combined ToF SIMS/XPS Study of Plasma Modification and Metallization of Polyimide. *Surf. Interface Anal.* **1999**, *27*, 609–617.
- (24) Wagner, A. J.; Wolfe, G. M.; Fairbrother, D. H. Reactivity of Vapor Deposited Metal Atoms with Nitrogen Containing Polymers and Organic Surfaces Studied by in Situ XPS. *Appl. Surf. Sci.* **2003**, *219*, 317–328.
- (25) Rastomjee, C. S.; Keil, M.; Sotobayashi, H.; Bradshaw, A. M.; Lamont, C. L. A.; Gador, D.; Umbach, E. Aluminium Metallisation of Argon and Oxygen Plasma Modified Polycarbonate Thin Film Surfaces. *Appl. Surf. Sci.* **1998**, *136*, 280–297.
- (26) Sang, L.; Pemberton, J. E. Penetration and Reaction Depths of Vapor Deposited Ag, Mg, Al, and Ca on Oligothiophene Thin Films. *Chem. Mater.* **2019**, *31*, 6908–6917.
- (27) Sang, L.; Pemberton, J. E. Chemistry at the Interface of α Sexithiophene and Vapor Deposited Ag, Al, Mg, and Ca: A Molecular View. *J. Phys. Chem. C* **2019**, *123*, 18877–18888.
- (28) Walker, A. V.; Tighe, T. B.; Cabarcos, O.; Haynie, B. C.; Allara, D. L.; Winograd, N. Dynamics of Interaction of Magnesium Atoms on Methoxy Terminated Self Assembled Monolayers: An Example of a Reactive Metal with a Low Sticking Probability. *J. Phys. Chem. C* **2007**, *111*, 765–772.
- (29) Calderone, A.; Lazzaroni, R.; Brédas, J. L.; Le, Q. T.; Pireaux, J. J. The Aluminum/Polyethylene Terephthalate Interface: A Joint Theoretical and Experimental Study. *J. Chem. Phys.* **1995**, *102*, 4299–4307.
- (30) Psarellis, G. M.; Aviziotis, I. G.; Duguet, T.; Vahlas, C.; Koronaki, E. D.; Boudouvis, A. G. Investigation of Reaction Mechanisms in the Chemical Vapor Deposition of Al from DMEAA. *Chem. Eng. Sci.* **2018**, *177*, 464–470.
- (31) Aviziotis, I. G.; Duguet, T.; Vahlas, C.; Boudouvis, A. G. Combined Macro/Nanoscale Investigation of the Chemical Vapor Deposition of Fe from Fe(CO)₅. *Adv. Mater. Interfaces* **2017**, *4*, 1601185.
- (32) Aviziotis, I. G.; Cheimarios, N.; Duguet, T.; Vahlas, C.; Boudouvis, A. G. Multiscale Modeling and Experimental Analysis of Chemical Vapor Deposited Aluminum Films: Linking Reactor Operating Conditions with Roughness Evolution. *Chem. Eng. Sci.* **2016**, *155*, 449–458.
- (33) Aufray, M.; André Roche, A. Epoxy–Amine/Metal Interphases: Influences from Sharp Needle like Crystal Formation. *Int. J. Adhes. Adhes.* **2007**, *27*, 387–393.
- (34) Aufray, M.; Roche, A. Properties of the Interphase Epoxy Amine/Metal: Influences from the Nature of the Amine and the Metal. *Adhesion Current Research and Applications*; Wiley, 2005; pp 89–102.
- (35) Grunze, M.; Hähner, G.; Wöll, C.; Schrepp, W. Interphase orientation of polyimide on polycrystalline gold, silver and Si(100). *Surf. Interface Anal.* **1993**, *20*, 393–401.
- (36) Duguet, T.; Bessaguet, C.; Aufray, M.; Esvan, J.; Charvillat, C.; Vahlas, C.; Lacaze Dufaure, C. Toward a Computational and Experimental Model of a Poly Epoxy Surface. *Appl. Surf. Sci.* **2015**, *324*, 605–611.
- (37) Frisch, M. J.; Trucks, G. W.; Schlegel, H. B.; Scuseria, G. E.; Robb, M. A.; Cheeseman, J. R.; Scalmani, G.; Barone, V.; Petersson, G. A.; Nakatsuji, H.; Li, X.; Caricato, M.; Marenich, A. V.; Bloino, J.; Janesko, B. G.; Gomperts, R.; Mennucci, B.; Hratchian, H. P.; Ortiz, J. V.; Izmaylov, A. F.; Sonnenberg, J. L.; Williams Young, D.; Ding, F.; Lipparini, F.; Egidi, F.; Goings, J.; Peng, B.; Petrone, A.; Henderson, T.; Ranasinghe, D.; Zakrzewski, V. G.; Gao, J.; Rega, N.; Zheng, G.; Liang, W.; Hada, M.; Ehara, M.; Toyota, K.; Fukuda, R.; Hasegawa, J.; Ishida, M.; Nakajima, T.; Honda, Y.; Kitao, O.; Nakai, H.; Vreven, T.; Throssell, K.; Montgomery, J. A., Jr.; Peralta, J. E.; Ogliaro, F.; Bearpark, M. J.; Heyd, J. J.; Brothers, E. N.; Kudin, K. N.; Staroverov, V. N.; Keith, T. A.; Kobayashi, R.; Normand, J.; Raghavachari, K.; Rendell, A. P.; Burant, J. C.; Iyengar, S. S.; Tomasi, J.; Cossi, M.; Millam, J. M.; Klene, M.; Adamo, C.; Cammi, R.; Ochterski, J. W.; Martin, R. L.; Morokuma, K.; Farkas, O.; Foresman, J. B.; Fox, D. J. *Gaussian 09*, Revision D.01; Gaussian Inc: Wallingford CT, 2013.
- (38) Perdew, J. P.; Burke, K.; Ernzerhof, M. Generalized Gradient Approximation Made Simple. *Phys. Rev. Lett.* **1996**, *77*, 3865–3868.
- (39) Grimme, S.; Antony, J.; Ehrlich, S.; Krieg, H. A Consistent and Accurate Ab Initio Parametrization of Density Functional Dispersion Correction (DFT D) for the 94 Elements H Pu. *J. Chem. Phys.* **2010**, *132*, 154104.
- (40) Francl, M. M.; Pietro, W. J.; Hehre, W. J.; Binkley, J. S.; Gordon, M. S.; DeFrees, D. J.; Pople, J. A. Self Consistent Molecular Orbital Methods. XXIII. a Polarization Type Basis Set for Second Row Elements. *J. Chem. Phys.* **1982**, *77*, 3654–3665.
- (41) Frisch, M. J.; Pople, J. A.; Binkley, J. S. Self Consistent Molecular Orbital Methods 25. Supplementary Functions for Gaussian Basis Sets. *J. Chem. Phys.* **1984**, *80*, 3265–3269.
- (42) Weigend, F.; Ahlrichs, R. Balanced Basis Sets of Split Valence, Triple Zeta Valence and Quadruple Zeta Valence Quality for H to Rn: Design and Assessment of Accuracy. *Phys. Chem. Chem. Phys.* **2005**, *7*, 3297–3305.
- (43) Weigend, F. Accurate Coulomb Fitting Basis Sets for H to Rn. *Phys. Chem. Chem. Phys.* **2006**, *8*, 1057–1065.
- (44) Reed, A. E.; Weinstock, R. B.; Weinhold, F. Natural Population Analysis. *J. Chem. Phys.* **1985**, *83*, 735–746.
- (45) Triguero, L.; Pettersson, L. G. M.; Ågren, H. Calculations of Near Edge X Ray Absorption Spectra of Gas Phase and Chemisorbed Molecules by Means of Density Functional and Transition Potential Theory. *Phys. Rev. B: Condens. Matter Mater. Phys.* **1998**, *58*, 8097–8110.
- (46) Triguero, L.; Plashkevych, O.; Pettersson, L. G. M.; Ågren, H. Separate State Vs. Transition State Kohn Sham Calculations of X Ray Photoelectron Binding Energies and Chemical Shifts. *J. Electron Spectrosc. Relat. Phenom.* **1999**, *104*, 195–207.
- (47) Ljungberg, M. P.; Mortensen, J. J.; Pettersson, L. G. M. An Implementation of Core Level Spectroscopies in a Real Space Projector Augmented Wave Density Functional Theory Code. *J. Electron Spectrosc. Relat. Phenom.* **2011**, *184*, 427–439.
- (48) Geudtner, G.; Calaminici, P.; Carmona Espíndola, J.; del Campo, J. M.; Domínguez Soria, V. D.; Moreno, R. F.; Gamboa, G. U.; Goursot, A.; Köster, A. M.; Reveles, J. U.; Mineva, T.; Vásquez Pérez, J. M.; Vela, A.; Zúñiga Gutierrez, B.; Salahub, D. R. *DeMon2k. Wiley Interdiscip. Rev.: Comput. Mol. Sci.* **2012**, *2*, 548–555.
- (49) Flores Moreno, R.; Alvarez Mendez, R. J.; Vela, A.; Köster, A. M. Half Numerical Evaluation of Pseudopotential Integrals. *J. Comput. Chem.* **2006**, *27*, 1009–1019.
- (50) Calaminici, P.; Janetzko, F.; Köster, A. M.; Mejia Olvera, R.; Zuniga Gutierrez, B. Density Functional Theory Optimized Basis Sets for Gradient Corrected Functionals: 3d Transition Metal Systems. *J. Chem. Phys.* **2007**, *126*, 044108.
- (51) Dunning, T. H. Gaussian Basis Sets for Use in Correlated Molecular Calculations. I. The Atoms Boron through Neon and Hydrogen. *J. Chem. Phys.* **1989**, *90*, 1007–1023.

- (52) Williams, A. R.; deGroot, R. A.; Sommers, C. B. Generalization of Slater's Transition State Concept. *J. Chem. Phys.* **1975**, *63*, 628–631.
- (53) Chong, D. P. Accurate Calculation of Core Electron Binding Energies by the Density Functional Method. *Chem. Phys. Lett.* **1995**, *232*, 486–490.
- (54) Chong, D. P.; Hu, C. H.; Duffy, P. Accurate Density Functional Calculation of Core Electron Binding Energies with a Scaled Polarized Triple Zeta Basis Set. Twelve Test Cases and Application to Three C₂H₄O₂ Isomers. *Chem. Phys. Lett.* **1996**, *249*, 491–495.
- (55) Gavrielides, A.; Duguet, T.; Esvan, J.; Lacaze Dufaure, C.; Bagus, P. S. A Poly Epoxy Surface Explored by Hartree Fock Δ SCF Simulations of C1s XPS Spectra. *J. Chem. Phys.* **2016**, *145*, 074703.
- (56) Atanasoska, L.; Anderson, S. G.; Meyer, H. M., III; Lin, Z.; Weaver, J. H. Aluminum/polyimide Interface Formation: An X Ray Photoelectron Spectroscopy Study of Selective Chemical Bonding. *J. Vac. Sci. Technol.* **1987**, *5*, 3325–3333.
- (57) Bèbin, P.; Prud'homme, R. E. Comparative XPS Study of Copper, Nickel, and Aluminum Coatings on Polymer Surfaces. *Chem. Mater.* **2003**, *15*, 965–973.
- (58) Sacher, E. Fluoropolymer Metallization for Microelectronic Applications. *Prog. Surf. Sci.* **1994**, *47*, 273–300.
- (59) Haynes, W. *CRC Handbook of Chemistry and Physics*, 95th ed.; CRC Press, 2014; pp 9–49.
- (60) Tanuma, S.; Powell, C. J.; Penn, D. R. Calculations of Electron Inelastic Mean Free Paths. IX. Data for 41 Elemental Solids over the 50 eV to 30 keV Range. *Surf. Interface Anal.* **2011**, *43*, 689–713.
- (61) Evertsson, J.; Bertram, F.; Zhang, F.; Rullik, L.; Merte, L. R.; Shipilin, M.; Soldemo, M.; Ahmadi, S.; Vinogradov, N.; Carlà, F.; et al. The Thickness of Native Oxides on Aluminum Alloys and Single Crystals. *Appl. Surf. Sci.* **2015**, *349*, 826–832.
- (62) Alexander, M. R.; Thompson, G. E.; Zhou, X.; Beamson, G.; Fairley, N. Quantification of Oxide Film Thickness at the Surface of Aluminium Using XPS. *Surf. Interface Anal.* **2002**, *34*, 485–489.
- (63) Mantina, M.; Chamberlin, A. C.; Valero, R.; Cramer, C. J.; Truhlar, D. G. Consistent Van Der Waals Radii for the Whole Main Group. *J. Phys. Chem. A* **2009**, *113*, 5806–5812.
- (64) Cordero, B.; Gómez, V.; Platero Prats, A. E.; Revés, M.; Echeverría, J.; Cremades, E.; Barragán, F.; Alvarez, S. Covalent Radii Revisited. *Dalton Trans.* **2008**, 2832–2838.
- (65) Turova, N. Y.; Kozunov, V. A.; Yanovskii, A. I.; Bokii, N. G.; Struchkov, Y. T.; Tarnopol'skii, B. L. Physico Chemical and Structural Investigation of Aluminium Isopropoxide. *J. Inorg. Nucl. Chem.* **1979**, *41*, 5–11.
- (66) Calderone, A.; Lazzaroni, R.; Brédas, J. L. A Theoretical Study of the Interfaces Between Aluminium and Poly (Ethylene Terephthalate), Polycaprolactone, and Polystyrene: Illustration of the Reactivity of Aluminium Towards Ester Groups and Phenyl Rings. *Macromol. Theory Simul.* **1998**, *7*, 509–520.
- (67) Van de Walle, C. G.; Neugebauer, J. First Principles Surface Phase Diagram for Hydrogen on GaN Surfaces. *Phys. Rev. Lett.* **2002**, *88*, 066103.
- (68) Zhu, J. Y.; Liu, F.; Stringfellow, G. B. Dual Surfactant Effect to Enhance *p* Type Doping in III V Semiconductor Thin Films. *Phys. Rev. Lett.* **2008**, *101*, 196103.
- (69) Hirschfelder, J. O.; Linnett, J. W. The Energy of Interaction Between Two Hydrogen Atoms. *J. Chem. Phys.* **1950**, *18*, 130–142.
- (70) Wiberg, K. B.; Ellison, G. B.; McBride, J. M.; Petersson, G. A. Substituent Effects on O H Bond Dissociation Enthalpies: A Computational Study. *J. Phys. Chem. A* **2013**, *117*, 213–218.
- (71) Yao, X. Q.; Hou, X. J.; Jiao, H.; Xiang, H. W.; Li, Y. W. Accurate Calculations of Bond Dissociation Enthalpies with Density Functional Methods. *J. Phys. Chem. A* **2003**, *107*, 9991–9996.
- (72) Rao, B. K.; Jena, P. Evolution of the Electronic Structure and Properties of Neutral and Charged Aluminum Clusters: A Comprehensive Analysis. *J. Chem. Phys.* **1999**, *111*, 1890–1904.
- (73) Deshpande, M. D.; Kanhere, D. G.; Vasiliev, I.; Martin, R. M. Ab Initio Absorption Spectra of Al_{*n*} (*n* = 2 – 13) Clusters. *Phys. Rev. B: Condens. Matter Mater. Phys.* **2003**, *68*, 035428.
- (74) Cai, M. F.; Dzugas, T. P.; Bondybey, V. E. Fluorescence Studies of Laser Vaporized Aluminum: Evidence for a 3Π_u Ground State of Aluminum Dimer. *Chem. Phys. Lett.* **1989**, *155*, 430–436.
- (75) Yang, S. H.; Drabold, D. A.; Adams, J. B.; Sachdev, A. First Principles Local Orbital Density Functional Study of Al Clusters. *Phys. Rev. B: Condens. Matter Mater. Phys.* **1993**, *47*, 1567–1576.
- (76) Boman, M.; Stafström, S.; Brédas, J. L. Theoretical Investigations of the Aluminum/Polythiophene Interface. *J. Chem. Phys.* **1992**, *97*, 9144–9153.
- (77) Dannetun, P.; Boman, M.; Stafström, S.; Salaneck, W. R.; Lazzaroni, R.; Fredriksson, C.; Brédas, J. L.; Zamboni, R.; Taliani, C. The Chemical and Electronic Structure of the Interface Between Aluminum and Polythiophene Semiconductors. *J. Chem. Phys.* **1993**, *99*, 664–672.
- (78) Parenté, V.; Lazzaroni, R.; Selmani, A.; Brédas, J. L. A Density Functional Theory Study of the Aluminum/Polythiophene Interface. *Synth. Met.* **1994**, *67*, 147–150.
- (79) Lu, T.; Chen, F. Multiwfn: A multifunctional wavefunction analyzer. *J. Comput. Chem.* **2012**, *33*, 580–592.
- (80) Alexander, M. R.; Thompson, G. E.; Beamson, G. Characterization of the Oxide/Hydroxide Surface of Aluminium Using X Ray Photoelectron Spectroscopy: A Procedure for Curve Fitting the O 1s Core Level. *Surf. Interface Anal.* **2000**, *29*, 468–477.